Heat exchangers for thermoacoustic systems: A review

Md Arman Arefin, Islam Ramadan, Hélène Bailliet

Heat exchangers for thermoacoustic systems: A review

Md Arman Arefin[1*], Islam Ramadan[2], Hélène Bailliet[3]
[1,2,3]Institut Pprime, University of Poitiers, 86000 Poitiers, France

*Corresponding author email: md.arman.arefin@univ-poitiers.fr

Abstract

Thermoacoustic (TA) devices convert heat into mechanical work or provide cooling via acoustic field. Heat exchangers (HXs), which transfer energy to and from the internal components, must be optimally designed to ensure device performance. Although numerous studies on TA HXs have been conducted over the past few decades, the information remains scattered and poorly organized, making it difficult to assess progress. Moreover, there is no consensus on design rules, the choice of working fluid, or key heat transfer parameters. Therefore, the purpose of this review is to provide a structured overview of past developments, identify key gaps that require attention, and provide future guidelines. This review presents the development of TA HXs over the last 25 years, focusing on oscillating flow heat transfer correlations, parametric studies, and design considerations for efficient engines and refrigerators. The analysis highlights that considerable improvements have been made in the design and analysis of TA HXs, their heat transfer characteristics, and fabrication methodologies. However, many existing design methodologies are borrowed from steady flow applications, and optimizing individual parameters in isolation is often inadequate. Additionally, no comprehensive method exists to evaluate the effectiveness of TA HXs. To address these, the study recommends simultaneous consideration of HX length, porosity, fin spacing, separation gap, and HX effectiveness, which is not frequently tested in the literature. Finally, a similitude study is conducted to reduce the number of design parameters, simplify physical analysis, and propose a new correlation of Nusselt number for oscillating flow heat transfer.

Keywords: Heat exchangers, oscillating flow, thermoacoustic, heat transfer

Contents

Contents **1**

1 Introduction **4**

2 General review **8**

2.1 Popular types of HX 9

2.2 Performance parameters 10

2.3 Directly applicable design rules 13

2.4 Geometrical parameters 14

3 Review of recent literature focused on HX **19**

4 Discussion on heat transfer models **22**

4.1 Adapted from steady flow equations 22

4.2 Correlations developed for oscillating flow 23

5 Discussion on geometrical parameters **29**

5.1 Length of HX (L) and separation gap (g) 30

5.2 Effect of porosity (Φ) 32

5.3 Effect of hydraulic radius (R_h) 33

5.4 Effect of fin spacing (D or $2Yo$) or plate spacing (parallel plate HX) 34

6 Challenges **36**

6.1 Fabrication challenges 36

6.2 Turbulence 38

6.3 Challenges with numerical study 39

7 Similitude study for future research **40**

8 Conclusion **44**

References **46**

Roman Symbols

Symbol	Description	Unit
A	Cross-sectional area	m^2
a	Speed of sound	m/s
C_p	Specific heat of water	J/(kg·K)
D	Fin spacing	m
D_h	Hydraulic diameter	m
f	Frequency	Hz
F_L (or L)	Fin length	m
F_T	Fin thickness	m
F_w	Fin width	m
g	Separation gap	m
h	Convective heat transfer coefficient	$W/m^2.K$
L	Length	m
$\dot{m}$	Mass flow rate of water	kg/s
$\dot{m}_{\mathrm{osc}}$	Mass flow rate of the gas that oscillates between the HXs	kg/s
Nu	Nusselt number	–
P	Perimeter	m
Pr	Prandtl number	–
$\dot{Q}_{\mathrm{c}}$	Heat rate pumped from the cold side of the regenerator	W
$\dot{Q}_{\mathrm{h}}$	Heat rate pumped from the hot side of the regenerator	W
$\dot{Q}_{\mathrm{k1}}$	Conduction heat rate (stack + gas)	W
$\dot{Q}_{\mathrm{k2}}$	Heat rate conducted by the canister and insulating sleeve	W
$\dot{Q}_{\mathrm{load}}$	Heat rate extracted at a lower temperature	W
q'_{load}	Heat rate per unit length at a lower temperature	W/m
$\dot{Q}_{\mathrm{leak\_cold}}$	Heat rate from environment to the HX	W
$\dot{Q}_{\mathrm{leak\_hot}}$	Heat rate loss from HX to the environment	W
$\dot{Q}_{\mathrm{th}}$	Thermoacoustically activated hydrodynamic heat rate along the stack	W
Re	Reynolds number	–
R_h	Hydraulic radius	m
S_{gen}	Entropy generation	W/K
S_t	Strouhal number	–
T	Period of sound wave	s
T_1	Inlet water temperature	K
T_2	Outlet water temperature	K
T_c	Temperature of cold reservoirs	K
T_h	Temperature of hot reservoirs	K
V	Velocity amplitude	m/s
V_a	Valensi number	
$\dot{W}_{\mathrm{dis}}$	Acoustic power dissipation	W
$\dot{W}_{\mathrm{el}}$	Input electrical power	W
$\dot{W}_{\mathrm{ex}}$	Acoustic power loss in the heat exchanger	W
$\dot{W}_{\mathrm{res}}$	Acoustic power loss in the resonator	W
$\dot{W}_{\mathrm{tc}}$	Useful acoustic power for thermoacoustic process delivered to the core	W
$\dot{W}_{\mathrm{tot}}$	Total acoustic power	W
X_1	Particle displacement amplitude	m

Greek Symbols

Symbol	Description	Unit
β_r	Blockage ratio	–
γ	Ratio of isobaric to isochoric heat capacities	–
δ_k	Thermal penetration depth	m
δ_v	Viscous penetration depth	m
ε	Effectiveness	–
η_{ac}	Acoustic network efficiency	–
η_{elec}	Electroacoustic efficiency	–
k	Thermal conductivity	W/(m·K)
μ	Dynamic viscosity	kg/m.s
Φ	Porosity	–
ρ	Density of gas	kg/m^3
ω	Angular frequency	rad/s

Subscripts

Subscript	Description
A	Amplitude
c	Cold
H	Hot
g	Gas
s	Solid
ref	At reference temperature
rms	Root mean square

Abbreviations

Abbreviation	Description
BLC	Boundary layer conduction
CFD	Computational fluid dynamics
COP	Coefficient of performance
CHX	Cold heat exchanger
CHX	Hot heat exchanger
DR	Drive ratio
SW	Standing wave
TA	Thermoacoustic
TAR	Thermoacoustic refrigerator
TASFE	Time average steady flow equivalent
TAE	Thermoacoustic engine
TAC	Thermoacoustic core
TW	Travelling wave

1 Introduction

The studies of the TA phenomenon started in the 19th century when Rayleigh discovered that pressure waves can be amplified if they interact in phase with an oscillating heat flux [1] [2]. Potentially, heat can be converted into mechanical work by producing oscillations in the fluid-solid matrix interaction within a porous material when a specific temperature gradient is imposed. Inversely, a cooling effect can be observed when gas oscillations are imposed on a porous material forming a temperature gradient. Besides, by using waste thermal energy, TA devices can be used for cooling purposes or to generate power [3][4][5]. This technique can potentially be competitive since it uses working fluids having no greenhouse effect, such as air, helium, argon, etc., and has lower maintenance expenses because of having limited number of moving components [6].

The terms "thermoacoustic engines" (TAEs) and "thermoacoustic refrigerators" (TARs), based on thermodynamic cycles, are two distinct classifications for TA devices. On the other hand, based on the phase lag between temperature and displacement, these devices are also divided into two categories [7]. For standing wave (SW) devices, the acoustic power delivered or produced via the thermodynamic cycle is lower than in traveling wave (TW) devices because the time phase shift between the acoustic velocity and pressure is $\sim 90^\circ$ for the SW and $\sim 180^\circ$ for the TW. This phase relationship is associated with the Brayton-like cycle for SW devices and with the Stirling-like cycle for TW devices. As in SW devices, the $\sim 90^\circ$ lag separates heat transfer from compression and expansion, resulting in alternating isobaric and isochoric steps similar to the Brayton cycle. Whereas in TW devices, the $\sim 180^\circ$ lag causes heat exchange during compression and expansion, producing nearly isothermal processes similar to the Stirling cycle.

HXs are essential components of TA systems. The first major step toward the use of HX was taken in 1962, led by Carter White, and Steele according to Avent and Bowen [8]. They demonstrated that the proper use of HXs can enhance energy conversion of a Sondhauss tube. After that, during the 1980s, a few researchers [9] [10] from Los Alamos National Laboratory refined the concept of HX to be integrated into practical TA devices. They developed HXs, which were placed adjacent to the stack/regenerator to have a controlled temperature gradient. The authors also tried to minimize viscous and thermal losses, emphasizing on optimized geometry, flow channel, etc. Later, many researchers worked on different types of HXs for TA systems starting from the early 2000s and conducted research on the optimization methodology, flow and heat transfer characteristics, etc. These collective efforts have gradually shaped the current state of TA HXs development and continue to guide ongoing research in the field, that will be discussed in the following.

Achieving an optimum HX design is essential for improving the efficiency of TA devices

[10]. However, their design has been a persistent technical and engineering challenge. This difficulty arises from the oscillatory nature of the flow, rendering existing knowledge applicable to steady flow arrangements of little practical value. Consequently, conventional heat transfer correlations developed for steady flows to the HX are debatable, leaving a gap in reliable and unequivocal design criteria, though these correlations are still useful for the design of practical TAEs and TARs. When designing effective HXs for transferring a specified heat load, it is primarily essential to optimize all the parameters associated to it. This optimization serves the following purposes:

- Ensuring the heat transfer surface area is favorable to minimize acoustic power loss caused by thermal and viscous dissipation.
- Ensuring the temperature drop between the HX and the adjacent fluid is compatible with minimal thermal irreversibility (minimizing the loss of usable energy during heat transfer between the HX and the adjacent fluid) [11][12].
- Extract or transport as much heat as necessary from inside or outside the device.

In the last couple of decades, several works have been done on TA devices. Table 1 highlights the major review works on TA systems for the last ten years. Reviews were conducted focusing on different aspects of TA devices such as experimental prototypes [5], optimization of different components [13][14][15][16], multi-physics coupling [17], performance analysis [18][19], numerical investigation [20], unconventional working fluid [21], categorizing TAR [22], and advances and challenges of TA technology [23]. However, to the best of the author's knowledge, no comprehensive review has been conducted on HXs that extensively addresses their progress, development, parametric optimization, and performance analysis. Although several numerical and experimental studies are found in the literature on the design, construction, performance, and development of HXs, the information is scattered, and due to that, the development is difficult to track. Therefore, keeping that in mind, this review tries to summarize the available information and combine them in a single source. Various aspects and parameters of the HXs, complexities, problem-solving methodologies, developments, and prospects are discussed and analyzed. Besides, some constructive recommendations are provided for future research and better understanding throughout the paper.

Table 1: **Summary of review articles published on TA systems in the last 10 years**

Ref	Year	Focus	Primary topics covered	Recommendations or findings
[5]	2015	TA prime movers and TAR	- Evaluating experimental prototypes	- Integration of high-intensity acoustic systems and components - Novel structures - high-pressure ratio, and power output (TA prime movers) - Multi-stage self-matching traveling wave TA devices are very promising
[13]	2015	TAR	- Focused on studies with highest temperature difference across the stack - Lowest acoustical work for cooling - Highest coefficient of performance (COP)	- Frequency and pressure are interdependent variables - When using gas mixtures, their percentage contribution should be monitored
[14]	2017	TAR	- Concept of TAR systems - Optimization techniques - Stacks and resonator tube design	- More improvement is needed on TA HXs - Found that TARs are likely to be lightweight and compact
[15]	2017	TAR	- General review: stack, working gas, resonator tube, optimization methods	- Stack position from the driver end should be optimized - Mylar is comparatively the most efficient stack material
[16]	2018	TAR	- Recent developments of TAR - Summary of optimization targets	- Multistage systems can achieve higher efficiency - Double loop-type TAR enhances efficiency and achieves low temperature oscillations - For single/double stage TARs, shorter regenerator helps in achieving reduced resistance
[17]	2021	TAR, TAE, TEG	- Multi-physics coupling effects - Prospects of coupling	- Active and passive acoustic-mechanical optimization approaches - Transducer choice depends on electromagnetism or piezoelectricity - Multi-objective optimization yields optimal solutions
[18]	2021	TA Stirling engines	- Investigate components - Engine performance	- Component dimensions/locations influence performance - Increasing number of regenerators increases performance

Ref	Year	Focus	Primary topics covered	Recommendations or findings
[20]	2022	TAR and TAE	- Numerical models	- Only linear porous-media model was found for stack, regenerator, and HX - Choice of turbulence model requires further study
[21]	2023	TAR and TAE	- Unconventional working fluids - System performance	- Liquid TA devices can use compact HX - Transcritical fluids can generate large pressure amplitudes - Two-phase TAE can operate at very low temperature differences - Solid TA is a new concept
[24]	2024	TAE	- Utilization and suppression of TA effect - Potential growth and application directions	- Phase-change processes and multi-stage design can reduce onset TAE temperature - Many applications identified - Carbon-based TA loudspeakers have large potential
[19]	2024	TAR and TAE	- Working mechanism and performance-affecting parameters - Commercial implementation	- Widespread deployment is stalled by technological immaturity - Linear models are not effective at high power density and amplitude - Computational fluid dynamics (CFD) modelling is valuable for addressing nonlinearities
[25]	2025	TAR	- Design and manufacture	- Porous ceramics for stacks provide durability - Graphene-coated copper for HX provides high thermal conductivity - Acoustic losses and scalability remain main challenges
[23]	2025	TAE	- Experimental setup and numerical analysis - Nonlinear effects in TA	- TAE technology has made considerable advancements - Future research should prioritize optimizing core engine components
[22]	2025	Heat-driven TAR	- Categorizing heat-driven TAR based on configurations: either SW or TW refrigerators, driven by either SW or TW engines	- Identified four fundamental categories

In this article, Section 2 provides an overview of TA HXs, including their types, key geometrical and performance parameters, design rules, and major contributions from the past

25 years. The aim of this Section is to introduce the commonly used HX configurations, outline the fundamental parameters governing their operation, and summarize research where any part of HXs has been investigated to understand the working environment of different research conducted. Section 3 focuses specifically on studies dedicated solely to TA HXs, highlighting recent advancements, key findings, assumptions, limitations, and offering recommendations for future work. Section 4 reviews heat transfer models and correlations (which are introduced in Section 2), both those adapted from steady flow applications and those developed for oscillating flows, with emphasis on their assumptions, applicability, and limitations. Section 5 examines the influence of critical geometrical factors, such as length, porosity, hydraulic radius, and fin spacing (which are introduced in Section 2) on HX performance and optimization. Section 6 discusses few broader issues, such as design challenges, fabrication constraints, and existing research gaps focusing on dynamics of flow and numerical analysis, along with recommendations to address them. Finally, Section 7 introduces a similitude study, proposing essential design parameters and structuring a new heat transfer correlation to support future development in TA HX's design and analysis.

2 General review

This Section gives an overview of TA HXs, starting from the presentations of some types (Subsection 2.1) of HXs. Further, in Subsection 2.2, the general performance parameters are discussed, taking a global view of the device performance and also a more local view of the performance of convective heat transfer, and in the next Subsection 2.3, some directly applicable design rules are mentioned. Finally, the important geometrical parameters are introduced to better understand the optimization properties discussed in later Sections of the paper.

A typical TAR or TAE is composed of several key elements, including a resonator or acoustic network, an acoustic driver or transducer, at least two HXs, and either a stack (in SW systems) or a regenerator (in TW systems). The stack or regenerator serves as the core component where the conversion between thermal and acoustic energy occurs. Regenerators are usually composed of materials like wire mesh, stacked spheres, or ceramic honeycomb shapes that minimize flow resistance while offering a wide surface area. The HXs are generally divided into a hot heat exchanger (HHX) and a cold heat exchanger (CHX), positioned on opposite sides of the stack or regenerator [26]. The HXs allow thermal communication with external heat sources and sinks by absorbing or supplying heat from their respective ends. The HXs are commonly built with parallel plates, finned surfaces, or compact tubular arrangements, etc. They function by continually exchanging heat between the gas and solid surfaces. In this sense, stacks and regerators are considered as HX because their primary

function is direct heat transfer between the gas and the solid. The main difference between stack/regenerator and the TA HXs is that the latters transfer the heat from/to a secondary fluid making the thermal link with external heat source/sink. Figure 1 below shows the schematic illustration of a SW TAR, highlighting the HXs and the stack.

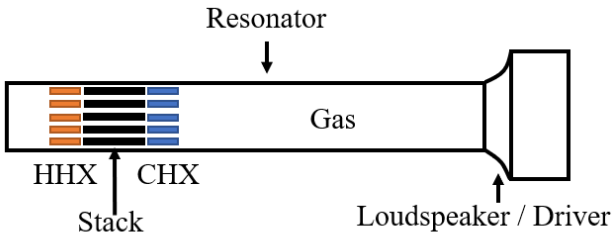

Figure 1: Schematic illustration of a SW TAR, highlighting HXs and stack.

2.1 Popular types of HX

The HXs are used to transfer the heat from/to the oscillating flow to a secondary flow which is generally water. To date, researchers have designed and analyzed several types of HXs that are used in oscillating flow. However, none of these are specifically designed for oscillating flow, rather many design rules are adapted from steady flow. Figure 2 shows different geometries encountered in TA devices. In the case of finned tube HXs (Figure 2 (a)), copper sheets are typically used to make the fins. Each fin has a hole bored through it so that copper tubes carrying water can pass through. Fins are assembled with the tubes and exterior copper casing after being cut to the proper length. In most cases, parallel plate HXs are generally built with simple parallel plates with a small space between them (Figure 2 (b)). The working fluid passes through the outer shell covering the plates. The heat transfer between the plates is facilitated by the gap, which enhances the interaction between the plates and acoustic waves, which is essential for TA phenomena. Besides, constructed as tightly coiled, helical tubes, spiral coil HXs provide a compact design for heat transfer, usually composed of aluminum or copper, two elements with high heat conductivity (Figure 2 (c)). However, the heat transfer surface area of this type of HXs is usually less than the other two types. Figure 2 (d) shows a shell and tube HX designed by [27]). A rectangular cross-sectioned peripheral canal supplies water to five tubes. Improved heat exchange between the water and the metal of the HX is achieved by orienting the HX radially with regard to the water inlet. This increases the water flow length inside the HX. With the application of electric discharge machining technology, the fins exposed to the oscillating gas were formed, increasing the heat transfer surface area on the gas side. Further, in recent year, a novel printed circuit HX was designed and fabricated by Wand and Hu [28]. The HX was made

of stainless steel plates with channels etched in. In this way, HHE, stack, and AHE can be integrated into one printed circuit HX.

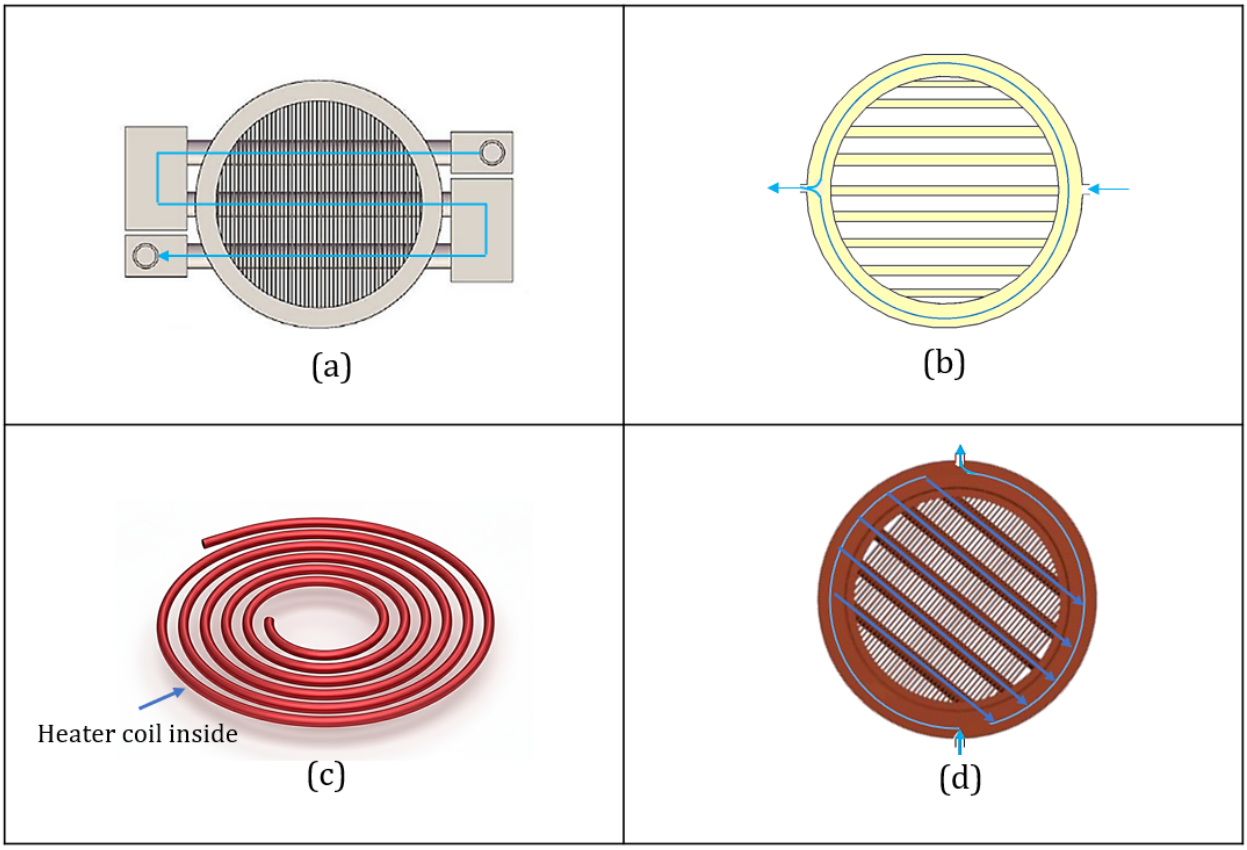

Figure 2: (a) Finned tube HX [29] (Reused with permission), (b) Parallel plate HX [30], (c) Spiral coil HX [31], (d) Shell and tube HX [27]. Here, blue lines represent secondary flow path.

This Subsection briefly addressed a few widely used HXs for TA systems. In the later Sections, a detailed analysis and discussion have been conducted related to these HXs.

2.2 Performance parameters

This Subsection introduces the key performance parameters of a TA device to highlight the importance of HXs. It also introduces various heat transfer related parameters of HXs, which are further analyzed in later Sections.

The performance of the HX influences the overall efficiency of a TA device. To further investigate the energy rates of a TAR, let us follow Wetzel and Herman [32], who stated that a TAR's COP is determined by the operation of its four main parts: the HX, the thermoacoustic core (TAC), the resonance tube, and the acoustic driver. The COP of a TAR is expressed as follows:

$$\mathrm{COP} \equiv \frac{\dot{Q}_{\mathrm{load}}}{\dot{W}_{\mathrm{el}}}, \tag{1}$$

where $\dot{Q}_{\mathrm{load}}$ is the heat load supplied to the CHX. The acoustic driver transforms the electric power input $\dot{W}_{\mathrm{el}}$ that is added to the system into total acoustic power $\dot{W}_{\mathrm{tot}}$. The electroacoustic efficiency, η_{elec}, for this energy conversion can be described as follows:

$$\eta_{\mathrm{elec}} \equiv \frac{\dot{W}_{\mathrm{tot}}}{\dot{W}_{\mathrm{el}}} = \frac{\dot{W}_{\mathrm{tc}} + \dot{W}_{\mathrm{dis}}}{\dot{W}_{\mathrm{el}}} = \frac{\dot{W}_{\mathrm{tc}} + \dot{W}_{\mathrm{res}} + \dot{W}_{\mathrm{ex}}}{\dot{W}_{\mathrm{el}}}, \tag{2}$$

where $\dot{W}_{\mathrm{tot}}$ is referred as the total acoustic power which is a combination of dissipated power $\dot{W}_{\mathrm{dis}}$, and $\dot{W}_{\mathrm{tc}}$ refers to the useful power for TA process delivered to the core. The component $\dot{W}_{\mathrm{dis}}$ in Equation 2 describes how the acoustic power dissipates in the device due to acoustic losses ($\dot{W}_{\mathrm{res}}$ and $\dot{W}_{\mathrm{ex}}$ are acoustic power loss in the regenerator and HX). Further, the acoustic network efficiency η_{ac} is introduced and defined as Equation 3.

$$\eta_{\mathrm{ac}} = \frac{\dot{W}_{\mathrm{tc}}}{\dot{W}_{\mathrm{tot}}}. \tag{3}$$

Further, the TA heat pumping at the regenerator can be defined as Equation 4, where $\dot{Q}_{\mathrm{c}}$ is the heat rate pumped from the CHX.

$$\mathrm{COP}_{\mathrm{TAC}} = \frac{\dot{Q}_{\mathrm{c}}}{\dot{W}_{\mathrm{tc}}}. \tag{4}$$

The effectiveness (ε) of the HX is defined as:

$$\varepsilon = \frac{\dot{Q}_{\mathrm{load}}}{\dot{Q}_{\mathrm{c}}}. \tag{5}$$

Combining all the above discussions, the COP of the TAR can be defined as Equation 6 (see Figure 3).

$$\mathrm{COP} = \eta_{\mathrm{elec}}\, \varepsilon\, \eta_{\mathrm{ac}}\, \mathrm{COP}_{\mathrm{TAC}}. \tag{6}$$

Hence, the overall COP for the TAR attains its peak, aligning with the core's thermoacoustic $\mathrm{COP}_{\mathrm{TAC}}$, when both efficiencies η_{elec} and η_{ac}, along with the ε, simultaneously achieve their optimal value of unity.

Besides, the heat rate transferred to/from the HX is an important parameter of analysis. Generally, in a TA system, the heat transfer rate of the CHX is calculated using Equation 7, where $\dot{m}$, C_p, T_1, and T_2 are the mass flow rate, specific heat, inlet, and outlet temperatures of the secondary fluid (e.g. water), respectively.

$$\dot{Q}_{\mathrm{load}} = \dot{m} C_p (T_1 - T_2). \tag{7}$$

The measured heat rate ($\dot{Q}_{\mathrm{h}}$) of the HHX is comprised of five different contributions as expressed by Equation 8, namely: $\dot{Q}_{\mathrm{c}}$, $\dot{Q}_{\mathrm{th}}$, which is the thermoacoustically activated hydrodynamic heat rate along the stack; $\dot{Q}_{\mathrm{k1}}$, the conduction heat rate transported by the solid portion of the stack and the gas; $\dot{Q}_{\mathrm{k2}}$, the heat rate conducted by the canister and further by the insulating sleeve, and finally, $\dot{Q}_{\mathrm{leak\_cold}}$, and $\dot{Q}_{\mathrm{leak\_hot}}$ which describe the loss of heat to/from the HX from/to the environment. Therefore, considering the HHX and CHX as a control volume (rather than the system's overall perspective), the heat balance becomes:

$$\left.\begin{aligned} \dot{Q}_{\mathrm{h}} &= \dot{Q}_{\mathrm{c}} - \dot{Q}_{\mathrm{leak\_hot}} - \dot{Q}_{\mathrm{k1}} - \dot{Q}_{\mathrm{k2}} + \dot{Q}_{\mathrm{th}}, \\ \dot{Q}_{\mathrm{c}} &= \dot{Q}_{\mathrm{load}} + \dot{Q}_{\mathrm{leak\_cold}} + \dot{Q}_{\mathrm{k1}} + \dot{Q}_{\mathrm{k2}}. \end{aligned}\right\} \tag{8}$$

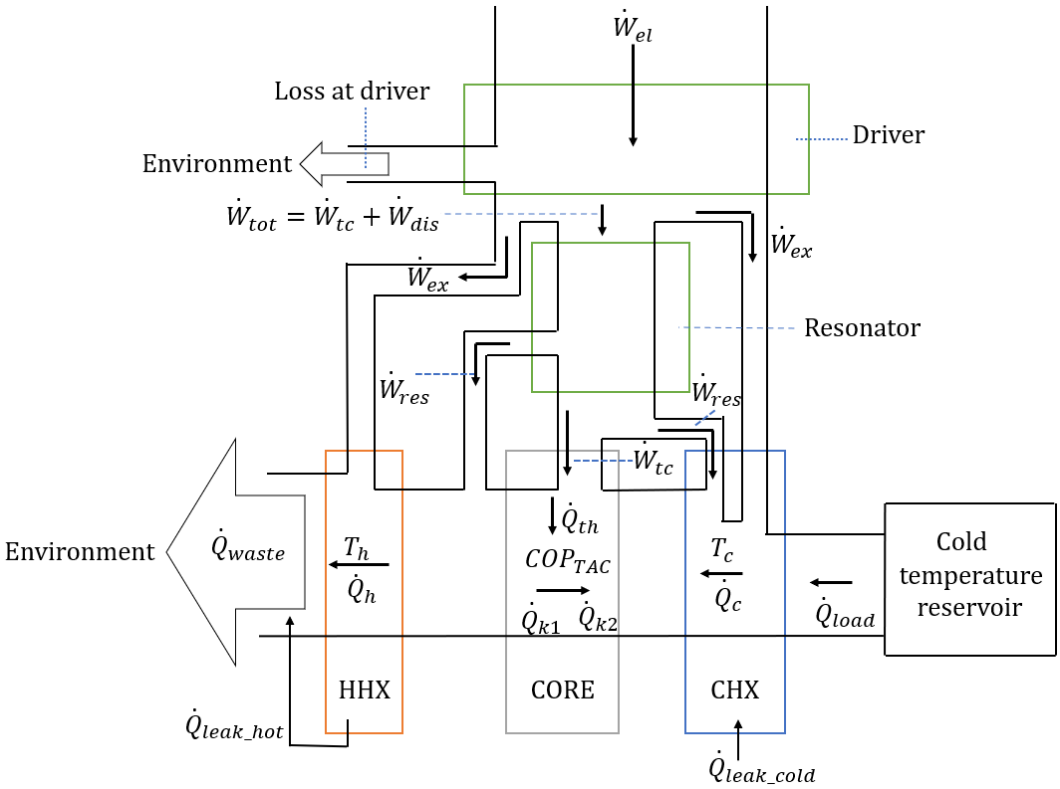

Figure 3: Graphical representation of the different heat rates. Adapted from [32].

Another key performance parameter of TA HX is the Nusselt number (Nu), which characterizes the balance between convective and conductive heat transfer. A higher Nu indicates dominance of convection, enhancing heat exchange with the working fluid. The commonly used regression takes the form:

$$Nu = Nu(Re, Pr), \tag{9}$$

where Re and Pr are the Reynolds and Prandtl numbers, respectively. Since this re-

gression is adapted from steady flow conditions, it is system specific and not universally applicable, as discussed further in detail in Sections 4.

This Subsection introduced the fundamental performance parameters needed to evaluate a TA HX. It was found that $\dot{Q}_{\text{load}}$, Nu, and ε are the performance parameters that are crucial for the analysis of HXs. Therefore, these parameters are further analyzed in depth in the later Sections 3, 4, and 5.

2.3 Directly applicable design rules

Historically, equipment or systems that transform energy into useful work have been assessed using the first law of thermodynamics, where efficiency is defined as the ratio of useful energy output (as work or heat) to the total energy input. Nonetheless, second law analysis has drawn more attention later as this technique shows how well the available energy is utilized of. The goal of the second law analysis is to minimize the entropy generation to optimize the design or operating conditions of HX [33]. Particularly in non equilibrium situations, entropy generation can be quantified by fusing the first and second laws of thermodynamics. These methods are different from just measuring the availability or irreversibility since those measure only indicate the amount of potential work lost. Alfred [34] analyzed a TAE working as a heat pump. The author applied the first and second laws in a control volume containing the heat pump. The first law can be written as:

$$\dot{Q}_h - \dot{Q}_{\text{load}} - \dot{W}_{\text{el}} = 0. \tag{10}$$

The second law of the system can be written as:

$$\frac{\dot{Q}_h}{T_h} - \frac{\dot{Q}_{\text{load}}}{T_c} = \sum_i S_{\text{gen},i}, \tag{11}$$

where $\sum_i S_{\text{gen},i}$ is the entropy generated in the system at all steps i, and T_h and T_c are the temperatures of the hot and cold reservoirs. Combining Equations 10, and 11 and eliminating $\dot{Q}_h$, the COP of the heat pump is:

$$COP = \frac{\frac{T_c}{T_h - T_c}}{1 + \frac{T_h T_c}{(T_h - T_c)} \frac{\sum_i S_{\text{gen},i}}{\dot{Q}_{\text{load}}}}. \tag{12}$$

These expressions make it evident that decreasing entropy generation in a process is crucial for enhancing the overall performance of the device. Entropy generation within the regenerator Section is essential for the TA device's operation. At the plate surface of the HXs, heat is transferred between the gas and the plate. In such a process, entropy generation is inevitable. Therefore, the challenge of reducing entropy generation in HXs must be balanced with practical and economic design considerations. Besides, reducing it

will improve efficiency. Second law analysis helps to identify the optimal geometries for HXs within practical constraints.

In a TA HX, entropy generation occurs due to temperature and velocity gradients in the gas. These two factors significantly influence the overall entropy production. In narrow channels, velocity gradients dominate, leading to higher entropy generation. Conversely, in wider channels, temperature gradients become the primary contributor. This understanding highlights the importance of identifying an optimal channel width to minimize entropy generation.

Besides, based on literature, the working fluid is usually inert gases such as helium, argon, or air due to their favorable thermal conductivity and specific heat properties. Further, to analyze the thermal properties, two fundamental considerations are the thermal penetration depth $\delta_k = \sqrt{\frac{2k}{\rho C_p \omega}}$ and the viscous penetration depth $\delta_v = \sqrt{\frac{2\mu}{\rho\omega}}$ [35], where ρ is density, k is thermal conductivity, C_p is heat capacity, ω is angular frequency, and μ is dynamic viscosity. It is also mandatory to use materials with high thermal conductivity, such as copper and aluminum, for efficient heat transfer.

For the water circulation loop, the maximum cooling water velocity inside the pipes should be kept below a certain limit to avoid excessive noise and damage due to wear and tear of the pipes. Additionally, the water circulation system should be able to achieve the required water flow rate for the cooling system.

The common design models for TA devices [36][37] primarily focus on the other components (driver, stack, etc) rather than the HX. Despite the HX playing a crucial role in determining the device's COP, there is a lack of practical guidance for designing an appropriate HX.

This Subsection covered all the fundamental directly applicable design rules for TA HXs, which will be important to understand the later Sections 3, and 5. The understanding of entropy, δ_k, δ_v, and secondary flow is crucial for the later parts.

2.4 Geometrical parameters

In this Subsection, the main characteristics of the HX used in TA devices are discussed based on an analysis of the literature. Table 2 summarizes the relevant literature, to the best of our knowledge, where any part of the HX of the TA system (both engine and refrigerator) was partially taken into consideration in the last 25 years. According to the literature summarized in Table 2, the most discussed geometrical parameters of a TA HX are its length (L, along the guide axis), hydraulic radius (R_h), and porosity (Φ). The R_h is dependent on the configuration of the flow channel. For demonstration, a rectangular flow channel has been chosen. Besides, some other fundamental parameters are highlighted in Figure 4. Some important parameters such as fin length (F_L or L) (for finned HX, the fin length is

considered as HX length (L)) and fin thickness (F_T) are visible in the close up view. Φ in this article is defined as the ratio of the flow/gas cross-section area (A_g) to the total area (A). The inverse of porosity is defined as blockage. Further, another important parameter, separation gap (g) is defined as the distance between the stack and the HX in a TA device.

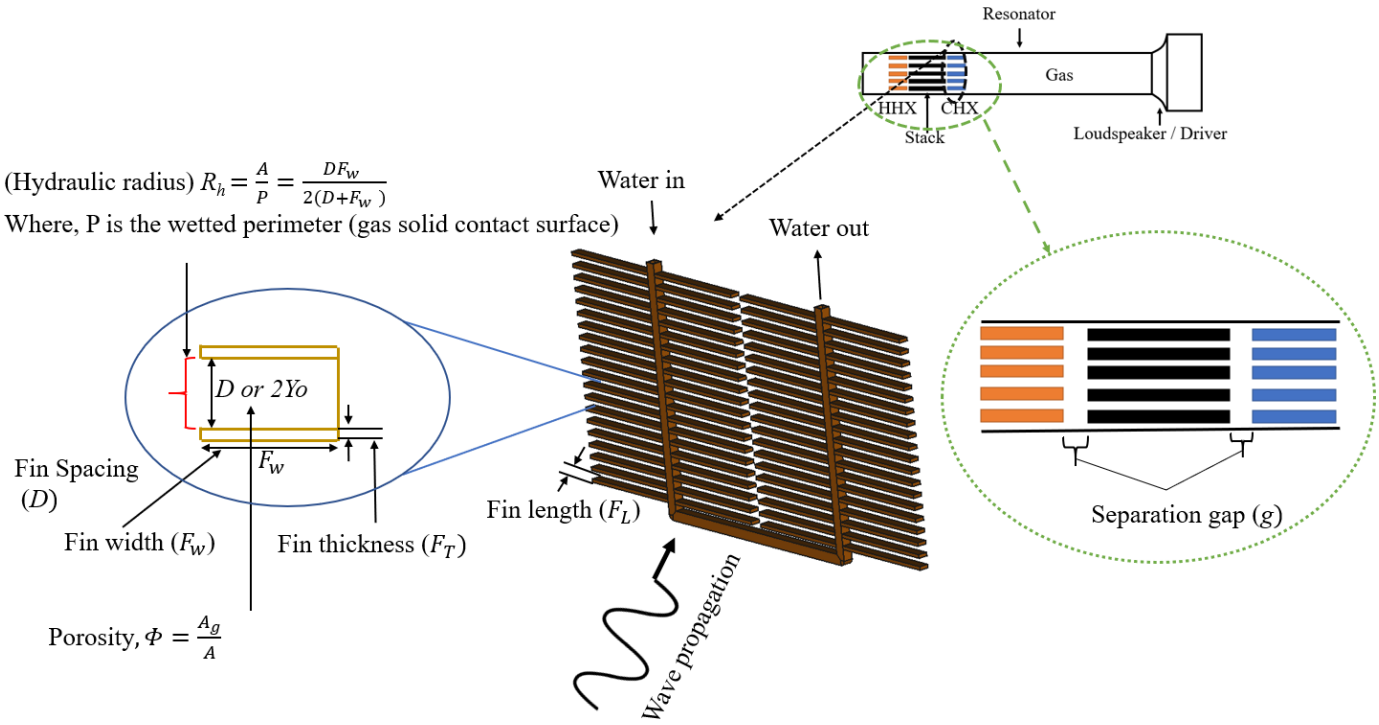

Figure 4: Magnified view of a finned tube HX.

It appears from the analysis of Table 2 that a good number of studies and in depth analyses focused on stack, resonator, HX, and loudspeaker. Note that studies solely focused on HXs are considered in Section 3, and a separate discussion is carried out for better understanding. Besides the reason of finding the fundamental design parameters, another purpose of Table 2 is to help readers understand the working environment and operating conditions of different research and experiments where any part of HX was evaluated.

Here, only the fundamental geometrical parameters of the HX are highlighted and introduced. A detailed discussion of each parameter and its optimization has been discussed in Section 5.

Table 2: Summary of previous work from 2000-2025, where the presence of HXs is considered.

Reference	**Method**	**HX Type**	**HX Length (hot and cold) (mm)**	**HX Fin Spacing/Plate Spacing (mm)**	**Porosity (%)**	**Working Fluid (inside resonator)**	**Stack Geometry**	**Frequency (Hz)**	**Resonator Type**	**Operating Pressure (bar)**
[35]	Experimental	Finned copper tubing	-	-	-	Air	Parallel fiberglass	42	-	3.0
[38]	Experimental	T/P	-	-	-	Air	Stack of plates	337	-	-
[39]	Experimental	T/P	-	-	-	He–Ar	-	100-200	$\lambda/2$	20
[40]	Experimental	T/P	-	-	-	He-Ar, He-Kr, and He-Xe	-	400	-	10
[41]	Theoretical	T/P	1.47	-	-	He	Parallel plates, circular pores, pin arrays, triangular pores	-	$\lambda/2$, $\lambda/4$	10
[42]	Experimental	T/P	-	-	-	Air	-	10-100	-	1.0
[43]	Numerical	T/P	-	-	-	-	Single plate	-	$\lambda/2$	-
[44]	Experimental	Parallel copper plates	-	0.8	-	-	-	5-70	$\lambda/2$	1.0
[45]	Experimental	Finned tube	6.6	0.95	-	He	-	300-450	$\lambda/4$	10
[46]	Numerical	T/P	3.66	-	-	Air	-	140	-	-
[47]	Experimental	T/P	5.9	-	-	He	Parallel plate	400	$\lambda/4$	10
[48]	Numerical	T/P	-	-	30	-	70	-	-	30
[49]	Numerical	T/P	-	-	-	Air	-	475	$\lambda/4$	-
[50]	Experimental	Copper mesh (rolled)	4.56	-	-	-	Parallel plate	-	$\lambda/4$	-
[51]	Experimental	Plate type	-	0.5	-	He	-	400	$\lambda/4$	10
[52]	Theoretical	T/P	Variable based on the working fluid	Variable based on working fluid	-	He, Air, He-Ne, He-Ar, He-Xe	-	Variable based on working fluid	$\lambda/2$	5.0
[53]	Experimental	-	-	-	-	Helium	Parallel plate	250-500	$\lambda/4$	3.0-6.0
[54]	Experimental	Finned tube	50	1.0	-	Ar, Ni, He, Ni-He	Parallel plate	-	-	11
[55]	Experimental	Tube only	-	-	-	Air, Ni	Drinking Pipette	300-600	$\lambda/2$	-
[56]	Experimental	Finned tube	-	6.0	-	-	-	13.1	$\lambda/4$	-
[57]	Experimental	Parallel plate	35	-	-	Ni	-	13.1	$\lambda/4$	-
[58]	Numerical	Parallel fin	-	-	-	He	Parallel plate	200	$\lambda/2$	-

Reference	Method	HX Type	HX Length (hot and cold) (mm)	HX Fin Spacing/Plate Spacing (mm)	Porosity (%)	Working Fluid (inside resonator)	Stack Geometry	Frequency (Hz)	Resonator Type	Operating Pressure (bar)
[59]	Numerical	Treated as porous media	10	-	-	-	Parallel plate	20	-	5.06
[60]	Experimental	T/P	5 and 8*	1.0	67	Ni	-	50	-	5.0
[61]	Theoretical	T/P	-	-	-	-	Circular holes, parallel plates, pin arrays	73.4	$\lambda/2$	1.0
[62]	Experimental	T/P	-	-	-	Air	Corning Celcor stack	350	$\lambda/4$	1.0
[63]	Theoretical	T/P	-	-	-	Helium	Parallel plate	593	-	1.0
[64]	Experimental	Finned tube	-	1.0	-	Ni	-	25-125	-	2.0-12
[65]	Experimental and Numerical	Parallel plate	-	6.0	-	-	-	13.1	-	-
[66]	Experimental	T/P	50 and 20*	-	-	Air	-	205	$\lambda/2$	-
[67]	Experimental	Finned Tube	-	0.7	-	He	Parallel plate	-	-	40
[68]	Experimental	Tube HX	10 and 5*	-	-	He	Parallel and spiral	460	-	1.0
[69]	Numerical	Parallel plate	20	-	-	He	-	57	$\lambda/2$	10
[70]	Numerical	Parallel plate	7.87-31.48	-	-	He	Parallel plate	-	1.0	-
[31]	Experimental	Spiral coil	-	-	-	He	Spiral	400	$\lambda/4$	10
[29]	Experimental	Fin and tube	20	0.7, 1.4, 2.1	-	He	Parallel plate	-	$\lambda/2$	-
[71]	Theoretical	Shell-and-Tube	20	-	-	He	-	84	-	31
[26]	Experimental	Circular pores and straight fins	10 and 20*	1.0	55	Air	Honeycomb stack	155	-	-
[72]	Numerical	Parallel Plate	-	6.0	-	Ni	-	13.1	$\lambda/4$	1.0
[73]	Experimental	Finned tube	20, 200*	1.0	-	Air	Parallel plate	80	-	-
[74]	Experimental and numerical	Flat and ogive edge shaped circular pore	28	-	24.31	He	-	53.6	-	1.0
[75]	Experimental	Finned tube	20	1.1	54	Air	Pores of squared shape/ honeycomb	143.2	-	-
[76]	Numerical	Finned tube	3.6 and 1.8*	4	-	Helium	Parallel plates	500	$\lambda/2$	10
[77]	Numerical	Parallel Plate	-	6, 4.5, 3	-	Ni	-	13.1	$\lambda/4$	-

Reference	**Method**	**HX Type**	**HX Length (hot and cold) (mm)**	**HX Fin Spacing/Plate Spacing (mm)**	**Porosity (%)**	**Working Fluid (inside resonator)**	**Stack Geometry**	**Frequency (Hz)**	**Resonator Type**	**Operating Pressure (bar)**
[78]	Experimental	Finned tube and Circular pore	20	1.1	54 and 33	Air	Honeycomb	143.2	$\lambda/2$	-
[27]	Experimental	Shell and tube	23	-	-	He-Ar	-	47	-	40
[79]	Experimental and numerical	Tube banks	142	-	-	Air and He	-	14.2	-	1.0
[80]	Experimental and numerical	Parallel plate	-	0.6	40	CO_2	Packed stainless steel woven mesh screen	121	$\lambda/2$	-
[28]	Experimental	Printed circuit	5	-	-	CO_2	Etched microchannels with semi-oval cross-sections	7.6	-	up to 200
[81]	Experimental and numerical	Microtube	-	-	-	Octafluoropropane (R-218)	Vacuum-jacketed microtube	-	-	3.43
[82]	Numerical (coupled TAR and TAE)	-	TAR 16.2 and 9.2*, TAE 18 and 55*	TAR 0.6 and 0.5, TAE 1.7 and 0.45	TAR 75 and 79, TAE 60	Air	Parallel plate	50	$\lambda/2$	10
[83]	Experimental	Heat pipe	8	-	42	Air	Square pores	109.2	-	1

here, '*' indicates a CHX in case of different lengths, '-'either the value is not mentioned or not considered, T/P – type not mentioned, but the presence of HX is considered to some extent.

3 Review of recent literature focused on HX

This Section reviews key studies that have specifically focused on TA HXs, including their design, analysis, and experimental methodologies. The main ideas and assumptions in these articles are critically evaluated. Furthermore, research gaps are identified, and recommendations are provided where applicable to guide future investigations.

In the most recent years, several studies have been conducted on the design and optimization of TA HXs. Some are focused on optimizing the F_L and D of finned tube HXs [84] [45] [74] [29] [11] [72]. Besides, other types of HXs such as circular pores, parallel plates, etc. have been analyzed to a certain extent [78] [26] [85].

Paek et al. [84] examined the HX's thermal performance in a TA cooler. The research encompassed the development of experimental procedures and computational techniques designed to assess oscillating flow heat transfer coefficients. Colburn J factor (defined as the ratio of the convective heat transfer coefficient to the mass flow rate and specific heat capacity of the fluid), or dimensionless heat transfer coefficients, were calculated using oscillating flow variables and then compared to steady flow measurement. The results were further compared with steady flow correlations and heat transfer coefficients were predicted by boundary layer conduction model that is further presented in Subsection 4.1. Precise predictions could not be obtained using a steady-flow correlation, and the boundary layer model which is frequently employed in TA computations failed to predict heat transfer coefficients and the effect of Re on heat transfer. Although the study recommended using time averaged steady flow equivalent equations (see Subsection 4.1) to predict convective heat transfer in HXs, it focused only on finned tube configurations. Therefore, other types of HXs, such as circular pore, shell and tube, and similar designs should be investigated under comparable working conditions to draw definitive conclusions.

Piccolo et al. [78] aimed to fill this gap while exploring the optimal geometrical configuration of the HX considering R_h, g, and Φ. In addition, the research highlighted the influence of the g, and Φ difference between HX and stack, overall emphasizing the need for an optimized relationship between these parameters. The study also focused on the gas side heat transfer coefficient calculation. The authors examined the performance of two types of HXs: finned tube and circular pore (in circular pore HX, instead of fin, simply circular pores are drilled along the guide axis). The circular pore HX was found to have lower performance than the former one, which is a clear indication of some acoustic loss mechanism. The authors predicted that though circular pore HX has a smaller heat transfer area compared to finned tube HX, the viscous dissipation occurring on the HX's surfaces could be partially responsible for the observed behavior. Authors predicted that in the circular pore HX, the larger pore sizes and surface interactions may lead to an increased $\frac{\delta_v}{\delta_k}$, intensifying viscous dissipation and

thereby reducing HX performance compared to the finned tube HX, where optimized fin geometry helps regulate this effect. However, this prediction may not be entirely accurate, as the ratio $\frac{\delta_v}{\delta_k}$ is actually $\sqrt{\mathrm{Pr}}$, which depends only on fluid properties and is independent of geometry. Therefore, for future study, it is recommended to investigate different circular pore HXs with varying pore size and flow regimes (i.e the article only considered laminar regime) to have a clear understanding of the loss mechanism.

For an enhanced thermal analysis, a symmetrical arrangement of three identical HXs was used in [74], with one HHX positioned in the middle between two CHXs. Both CFD and experimental studies were conducted by the authors to validate the results. The results suggest that the minor losses in the TA system are mainly driven by the drive ratio (DR, defined as the ratio of dynamic pressure amplitude and mean pressure). The authors noted that a minor drop in heat transfer performance occurs at a low drive ratio when profile edges (flat and ogive) are present. On the other hand, the effect gradually decreases as the DR rises, and the two edge shapes perform similarly at high amplitudes. Nonetheless, the computational analysis discovered that the ogive edge reduced flow velocity at the entrance and exit of the HX gas channels, hence minimizing vortex formation and shedding. This resulted in a notable decrease in pressure loss, particularly at high amplitudes. Thus, the study suggested that the overall performance of TA systems will be enhanced by (ogive) tube-HXs with profiled gas channels.

Kamsanam et al. [29] studied how D affects the finned tube HX's thermal performance. Under a variety of testing circumstances, the heat transfer rate between two finned tube HXs placed side by side in an oscillatory flow was studied. The ε of the HXs and heat transfer coefficient were calculated and discussed. Besides, as findings, the authors mentioned that with the increase of D, the heat transfer increases. The reason behind this conclusion is related to the increased Φ of the HXs, which fundamentally reduces minor losses. Besides, the authors also examined the ε of the HXs. As findings, it was reported that the HX having the largest D showed higher ε. However, at a $\frac{D}{\delta_k}$ (normalized fin spacing) near 2, the ε goes beyond 1, which is impractical. The reason behind this is probably due to the method used to calculate the maximum heat transfer rate which is given by $\dot{Q}_{\mathrm{load}} = \dot{m}_{\mathrm{osc}} C_p (T_h - T_c)$, where $\dot{m}_{\mathrm{osc}}$ is the mass flow rate of the gas that oscillates between the HXs. Further research is necessary to accurately define the maximum heat transfer rate, considering the gap between the two HXs. Additionally, the mass flow rate $\dot{m}_{\mathrm{osc}}$, as defined, may not fully reflect the behavior of oscillating flow due to differences in velocity and thermal boundary layer development compared to steady flow conditions.

Mahlalela et al. [86] investigated the influence of different blockage ratios (β_r) (28%, 36%, 42%, 47%, and 59%) of HX on the performance of a TAE. As key findings, the authors mentioned that efficiency is inversely correlated to onset temperature and directly to volu-

metric velocity. Authors also suggested that decreasing the β_r, decreases volumetric velocity and reduces efficiency, which is a direct contradiction to Kamsanam et al. [29], where their efficiency increased with increasing Φ. Further, the authors recommended an optimal β_r of 42% to 47%. Therefore, further studies are recommended to investigate the effect of Φ on CHX, considering also the F_T and F_L, as these factors may also influence the heat transfer behavior, which were not considered in these studies.

To study the thermal behavior of HXs and stack plates of TA devices, a simplified model of heat transfer was developed by Herman and Chen [87]. The authors reported that there is a minimal correlation between the HHX and CHX's thermal behaviors. This suggests that it is possible to analyze the CHX, and HHX's performances independently. However, this conclusion was made on the assumption that the behavior of HHX does not affect the behavior of CHX, which might not reflect the practical situation fully. Therefore, it is necessary to conduct experimental research separately on the HHX, and CHX to validate or counter the findings of this numerical research.

Saat and Jaworski [72] created a two dimensional ANSYS Fluent CFD model of flow over a pair of hot and cold HXs to interpret the unsteady characteristics of heat transfer phenomena observed in a previous study [56]. The simulated results demonstrated that the existence of temperature gradients modifies the velocity profiles within the HX plates, indicating intriguing modifications in the flow structure. The fluid and temperature profiles of the computer models and the experimental data follow a similar general pattern, however, with differences in magnitude particularly noticeable in the hot region, with a discrepancy of 30% with the experimental results, making it difficult to develop a concrete conclusion. The reason for this discrepancy can be that the geometry considered by the authors during CFD was an extreme simplification of the experimental geometry. Here, the authors only considered two plates of the HX, though the HX used in the experiment was geometrically more complex, changing the dynamics of flow and heat transfer characteristics.

Yang and Hu [88] used artificial intelligence with physical modeling for system optimization. In order to optimize the channel geometry inside the core of a supercritical CO_2 TAE, the authors presented a methodology that integrates deep reinforcement learning, artificial neural network-built surrogate models, and CFD simulations. The optimized channel design effectively balanced the heat transfer performance of the HHX, and CHX, resulting in a significant increase in the CHX's cooling capacity.

From the above discussion, it is visible that a considerable advancement has been made in understanding and optimizing the performance of HX for oscillatory flow conditions. Studies have demonstrated that the optimized geometry plays a vital role in minimizing acoustic losses and enhancing performance. The intricate relationships between flow dynamics and heat transfer have been identified through the use of CFD models and experimental con-

figurations; the outcomes of these efforts have led to proposals of new HX architectures. However, a large number of limitations can also be observed from the recent research: (a) one of the drawbacks is the heavy reliance on idealized models and design, and experiments limited by scale and the range of parameters tested, leaving a gap in our understanding of how different variables interact under diverse operational conditions; for instance, all the above mentioned studies discussed in this Section considered Re only up to the laminar region. (b) Further, the limited investigation of the long-term performance and robustness of HXs under repeated thermal cycling and acoustic stresses, which are frequent in real-world applications, is another noteworthy drawback. To overcome the first drawback, it is recommended to simplify the problem initially by examining a plate of HX and evaluating its heat transfer properties. Further, the system could be made complex by adding one more plate and differentiating the characteristics of fluid flow and heat transfer. Later, the system can be made more complex to a practical HX and compared. This way, the heat transfer characteristics of oscillating flow could be understood better, helping in designing efficient HXs for TA systems. Also, the ideal way of analyzing the geometrical parameters is to analyze L, Φ, and g simultaneously. Regarding the second issue, more research should be conducted under repeated thermal cycling and acoustic stresses, and on life cycle analysis and compare them to reach a definite conclusion. Finally, it is imperative to have clear and standardized design criteria, as existing guidelines sometimes lack consistency, leading to varying results across different studies.

4 Discussion on heat transfer models

This is a key point when reviewing works on HX in TA devices as a correct description of HX and especially of their performances relies on an accurate modeling of heat exchange between the fluid and the solid. This Section therefore reviews the existing models and makes it apparent that there is no consensus on the estimate of heat transfer coefficient in oscillating flow. For simplification, the Section is divided into two parts. Subsection 4.1 highlights the models adapted from steady flow equations, and 4.2 discusses the correlations developed from oscillating flow experiments. Further, recommendations are provided on selecting proper corelation based on Re of the flow.

4.1 Adapted from steady flow equations

The classical method of defining heat transfer through a HX is the boundary layer conduction (BLC) method developed by Swift [89]. Till date, this method is still widely used in TA and incorporated in DeltaEC [90] and it defines the heat transfer coefficient h with respect to thermal conductivity K as:

$$h = \frac{K}{\min(R_h, \delta_k)}. \tag{13}$$

Heat transfer correlations of the form $Nu = Nu(Re,\ Pr)$ in the traditional steady flow model are adapted to the case of oscillatory flows using the time average steady flow equivalent (TASFE) model [91]. This adaptation involves averaging these correlations over an acoustic cycle. In this process, the velocity represented in the Re of the steady flow correlation is assumed to be the velocity amplitude (V) and sinusoidally oscillating and is substituted in the conversion process as $V\sin(\omega t)$. Next, the resulting time dependent Nu is calculated as the time average over a half cycle.

$$Nu_{TASFE} = \frac{1}{T/2}\int_0^{T/2} Nu(Re\sin(\omega t), Pr)\, dt, \tag{14}$$

where T is the period of the acoustic wave, ω is the angular frequency, and t is the time.

Similarly, in the root mean square-Reynolds (RMS-Re) model [78], the Re appearing in the correlation of steady flow is substituted by particle rms (square root of the average of the squares of the speeds of gas molecules) velocity.

$$Nu_{rms} = Nu\left(\frac{Re_{rms}}{\sqrt{2}}, Pr\right). \tag{15}$$

All the above mentioned correlations are developed from steady flow and can not properly catch the behavior of oscillating flow heat transfer, therefore, are not widely used now in experimental research, except BLC. The BLC model remains in use because of its simplicity and reasonable accuracy in some conditions and it is also used as a benchmark for comparison with newer models.

4.2 Correlations developed for oscillating flow

In this Subsection, the various heat transfer correlations (the form was introduced in Subsection 2.2) developed by different authors through experimentation are gathered and evaluated. Besides, some recommendations are provided on the choice of proper correlations by the end of this Subsection.

Paek et al. [84] first experimentally proved that the steady flow equations are not applicable for oscillating flow and developed a heat transfer correlation for TA HXs using the Colburn J factor. Following the work, several researchers [45][92][78][29] conducted experiments and developed correlations for the oscillating Nu.

A finned tube aluminum HX with a fin spacing of 0.54 mm was investigated by Paek et al. [84]. The system was operated under three distinct mean pressures (20 bar, 13.3 bar, and 6.7 bar) and driven close to its resonant frequency (136–155.9 Hz). This HX was integrated

as CHX in a TA cooler that was filled with three He-Ar mixtures (44% He, 33% He, and 22% He). After converting the Colburn J factor to the Nu, the measurement's heat transfer correlation was found to be (where subscript A denotes that Re is calculated using velocity amplitude, and the characteristic length is R_h):

$$Nu = 1.303\, Re_A^{0.3201}\, Pr^{0.33}. \tag{16}$$

In equation 16, Re_A determines the relative importance of inertial to viscous forces in oscillating flow, which controls the convective mixing and heat transfer. Whereas Pr governs the relative rate of momentum and thermal diffusion. In TA devices, the choice of working gas mixture is driven by the aim to reduce viscous effects while promoting thermal exchange between the fluid and the solid; the Pr is a criteria for this goal. Correlation laws as Equation 16 permits to determine, for a given fluid, the evolution of the effectiveness of convective heat transfer with acoustic amplitude. It should be noted that compared to this initial definition of Nu number, additional effects such as end effects are also included in most of the system studied in the literature.

A copper parallel plate HX with 0.95 mm D, and 0.15 mm F_T was evaluated by Nsofor et al [45]. The device was operated at mean pressures between 3 bar and 8 bar and operation frequencies between 300 Hz and 450 Hz, and the TAR was loaded with He. Following the conversion of the Re_{rms} to the Re_A, the measurements' heat transfer correlation was found to be:

$$Nu = 0.548\, Re_A^{0.33}\, Pr^{0.11}. \tag{17}$$

Tang et al. [92] constructed an experimental setup that mimicked the pulse tube refrigerator's operational conditions in order to study the heat transfer capabilities of a copper finned HX that is cooled by water flowing through channels around it. The fins measured 20 mm in length in the direction of flow, 0.75 mm F_T, and 0.75 mm apart. At three mean pressures (25 bar, 30 bar, and 35 bar), He was the working gas, and the operating frequency ranged from 40 Hz to 110 Hz. The test findings were summed up as follows using the Valensi number (Va) and Re_A.

$$Nu = 0.43\, Re_A^{0.0876}\, Va^{0.475}, \tag{18}$$

$$Va = \frac{\rho_m \omega D_h^2}{\mu}. \tag{19}$$

Heat transfer measurements were conducted by Kamsanam et al. [67] on paired finned-tube HXs (without stack) positioned side by side in a He-filled resonator. Three copper HXs with F_L of 20 mm, F_T of 0.3 mm, and D of 0.7 mm, 1.4 mm, and 2.1 mm were examined.

Following the conversion of the Colburn J factor to the Nu, the correlation derived from the regression of their data is:

$$Nu = 0.203\, Re_A^{0.3606}\, Pr^{0.33} \left(\frac{F_T}{D_h}\right)^{-1.2541}. \tag{20}$$

Piccolo and Jaworski [78] did an experimental investigation with two types of HXs namely finned tube and circular pore. In the direction of flow, F_L was 2 cm. The HX itself was mechanically supported during its production by a 2 cm thick copper ring with an internal radius of 10.5 cm and an external radius of 14 cm. The cooling water travels through a 14 mm copper tube that has been crushed to create a rectangular cross-section pipe with an area of 2 cm by 0.5 cm, right outside the HX. The experiment was run at the resonance frequency of 143 Hz. The derived correlation was:

$$Nu = 0.47\, Re_A^{0.44}\, Pr^{\frac{1}{3}}. \tag{21}$$

Kamsanam et al. [29] did experimental research on a TA system with three HXs having different D of 0.7 mm, 1.4 mm, and 2.1 mm. The resonator was a half wavelength resonator, and the system was operated at resonance frequency. The derived correlations respectively for the three different D are:

$$Nu = 0.10\, Re_{rms}^{\frac{1}{3}}\, Pr^{0.71}. \tag{22}$$

$$Nu = 0.16\, Re_{rms}^{0.44}\, Pr^{0.70}. \tag{23}$$

$$Nu = 1.56\, Re_{rms}^{0.44}\, Pr^{0.34}. \tag{24}$$

The above discussion shows that the developed equations are system-specific, that is valid only for the system from which it was developed (Table 3). Also, all the correlations are valid only for the specific working fluid that was used during experiments. Therefore, it is necessary to reconsider the formulation of the Nu correlations, which is further considered in Section 7. However, with careful consideration, it is possible to generalize some of those for different Re_A and frequencies. Table 3 shows the Re_A range for a TA system and the corresponding suitable Nu equations. The errors are relative to the data provided by Piccolo and Jaworski [78] and are calculated based on the range of Re_A selected for them. Figure 5 was developed using different oscillating flow correlations and using data provided by Piccolo and Jaworski [78]. Note that for RMS-Re, and TASFE model, the Nu equation is adapted from the laminar steady flow equation. Figure 5 supports the recommendations made in Table 3. Nevertheless, considering a wide range of Re_A, the analysis shows that comparatively the most suitable correlations are BLC and the correlation developed by Tang

et al. [92]. The later is actually an approximate equation developed from BLC. However, note that BLC cannot predict the change of Nu with the change of Re_A .

Table 3: Recommended heat transfer correlations based on Re_A. Also, comparison among correlations developed for oscillating flow.

Correlation	**Ref.**	**Adaptability based on Re_A number**	**Mean Abs. % Error**	**Frequency (Hz)**	**Mean pressure (bar)**	**Assumptions**	**Limitations**	**Comments**
$1.303Re_A^{0.3201}Pr^{0.33}$	[84]	500 - 4000	27	Close to its resonant frequency (136–155.9)	20, 13.3, and 6.7	When peak to peak gas displacement is smaller than the HX length, the effective heat transfer area is perimeter multiplied by displacement amplitude	The equation was verified for upto Re_A 4000 and peak to peak particle displacement range varied from 2.5 mm to 5.3 mm	The modified TASFE model can be adapted to future research after verification
$0.548Re_A^{0.33}Pr^{0.11}$	[45]	0 - 150	12	300 - 450	3, and 8	Fin equation assumes heat conduction occurs only along the length of the fin. Also, the velocity equation assumes a lossless standing wave	Re was defined with rms velocity, and a single drive ratio (Dr 0.02) was considered	Effect of frequency on heat transfer was analyzed, which can be adapted in future research
$0.43Re_A^{0.0876}Va^{0.475}$	[92]	200 - 1200	24	40 - 110	25, 30, and 35	The temperature of the oscillating flow is taken as the average of the temperatures measured at both ends of the HX. 1D heat conduction was considered for fin efficiency calculation	Va range of 150 to 350 was considered. The equation has not been tested or validated for turbulent oscillatory flows or for higher pressure ratios.	More experiments can be conducted for higher Re and also considering geometrical variation of HX
$0.47Re_A^{0.44}Pr^{1/3}$	[78]	200 - 2000	Base data	Resonance frequency 143	-	For water side convective heat transfer coefficient calculation, the fin surface temperature was assumed to be similar to water temperature	The correlation has an R^2 value of 0.73, and all experiments were conducted at a fixed frequency	Finned tube HX was superior to circular pore design in the specific configurations
$\frac{K}{\min(R_h,\delta_k)}$	[89]	Any range	18	-	-	-	Adapted from steady flow	Good in providing an average value

Correlation	**Ref.**	**Adaptability based on *Re* number**	**Mean Abs. % Error**	**Frequency (Hz)**	**Mean pressure (bar)**	**Assumptions**	**Limitations**	**Comments**
$0.203 Re_A^{0.3606} Pr^{0.33} \left(\frac{t}{D_h}\right)^{-1.2541}$	[67]	Not qualified	78	Resonance frequency	Variable (max 40)	Experiments were conducted by setting two HXs side by side (no stack/regenerator). Also, the water side heat transfer was determined by steady flow experiments and was considered valid for oscillating flow conditions	Fin efficiency was adapted from the steady flow concept	Provides large error
TASFE	[91]	200 - 300	13	-	-	-	Adapted from steady flow	Better for low Reynolds number

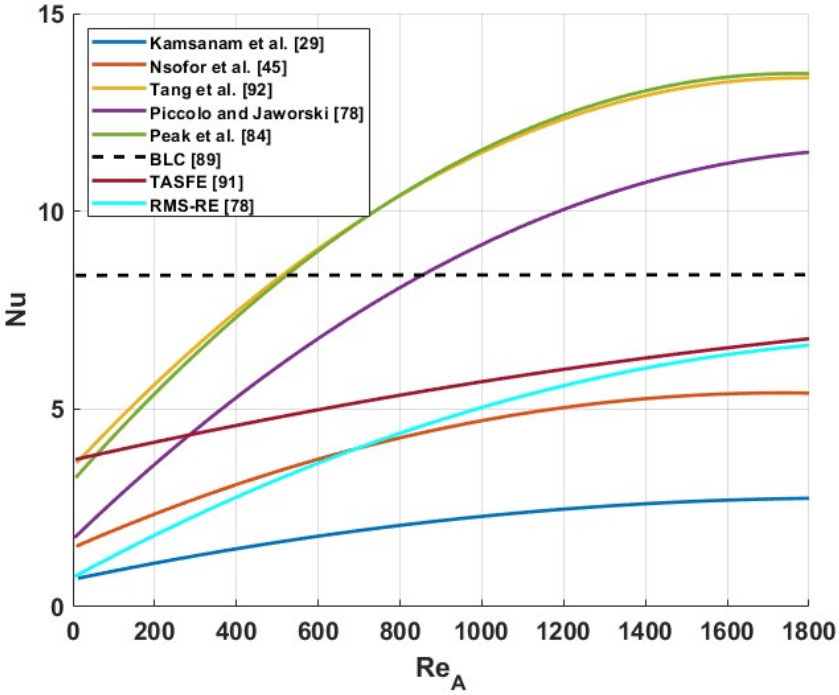

Figure 5: Nu based on Re_A using different correlations developed for oscillating flow (base data extracted from Piccolo and Jaworski [78].)

5 Discussion on geometrical parameters

This Section examines the geometrical parameters introduced in Section 2.4 and evaluates them in the context of optimizing the design of TA HXs. Recommendations are provided throughout the discussion.

Primarily in the TASFE model, and first and second law analyses, for simplicity, a single plate of an HX is considered. However, in practical cases, this assumption is not valid and there are more than one plate. All the available experimental work in the literature also considers HXs having multiple plates. Therefore, in this Section, discussions are carried out on practical HXs. Besides, from the above discussion of Section 2.4, four fundamental parameters are found: L, R_h, g, and Φ, which must therefore be set appropriately for the optimal design of TA HXs. Besides these general parameters, for finned tube HXs, F_T, F_L, and D are important for optimal design. Therefore, each of these parameters is discussed in this Section, summarizing the scaling rules given by previous researchers.

5.1 Length of HX (L) and separation gap (g)

Two important parameters in HX design are L, and g. g keeps the HHX from obstructing the regenerator/stack pores and reduces adverse thermal conduction from the HHX to the CHX in a TA device. As most of the recent studies conducted in the literature evaluated these two parameters simultaneously, therefore, in this Subsection, both are considered. To study the effect of CHX length (L_c) on the heat rate per unit length (q'_{load}), Piccolo [58] did a numerical study. To analyze the effect of L_c, simulations were performed at a fixed stack position and β_r, while varying the DR, D, and L_H. The author suggested that the cooling load increases quickly in the range of $0 < L_c < X_1$ (X_1 is the particle displacement amplitude) and becomes almost constant when $L_c > X_1$.

Further, in the earlier research, Swift [10] suggested that $L_c/2X_1 \approx 1$ is the optimum configuration for efficient interelement heat transfer. This result is supported by the claims that a particle can only transfer heat over a distance of $2X_1$, and that the total number of particles capable of taking part in interelement heat transfer is equal to the gas component contained within a distance of $2X_1$ from the stack edge. A similar observation was also claimed by Saat et al. [93], where the authors did a numerical study considering two plates. However, Swift [89] provided experimental evidence of improved engine performance with shorter HXs ($\approx X_1$) in a subsequent study. Swift's reasoning considers only the heat flux, but in practical application, the heat coming to the HX is not mainly due to heat transport; edge effects and other HX effects are also important. Further, even lower values of ($L_H/X_1 \approx 0.6$) of optimum length were found by Besnion and Knio [94]. The difference between Swift [89], Saat et al. [93], and Besnion and Knio [94] comes from the number of considered variables. Swift, and Saat et al. analyzed the L alone, where the former authors considered L and g together with drive ratio (DR). Besnion and Knio [94] found that the cooling load peaks at a particular g for a certain L_c. Similarly, the cooling load peaks at a predetermined L_c at a fixed g, as can be seen in Figure 6, which depicts that for all values of g, q'_{load} peaks at a well defined L_c. As observed, when deviating from the optimum length of the HX, the curves show a nearly sharp drop. A similar trend can be seen in the results obtained in [95], which was conducted at a low DR, where the value also decreases gradually.

Further, a numerical simulation of the flow in a Section of a half wavelength cooler was carried out by Marx and Blanc-Benon [96]. The authors numerically investigated HXs and zero-thickness stack plates, and to save computing costs, a high operating frequency was selected. The research primarily focused on how geometrical parameters affect the refrigerator's COP. The authors found that there is an optimum value of g to obtain a high COP and cooling power. The recommended g for a TAR is $0.2X_1$ to $0.4X_1$. Besnion and Knio [97] also suggested $0.40X_1$ as the g, noting that larger or smaller gaps than this drastically reduce cooling load. This occurs because X_1 limits the heat exchange between the HXs, and

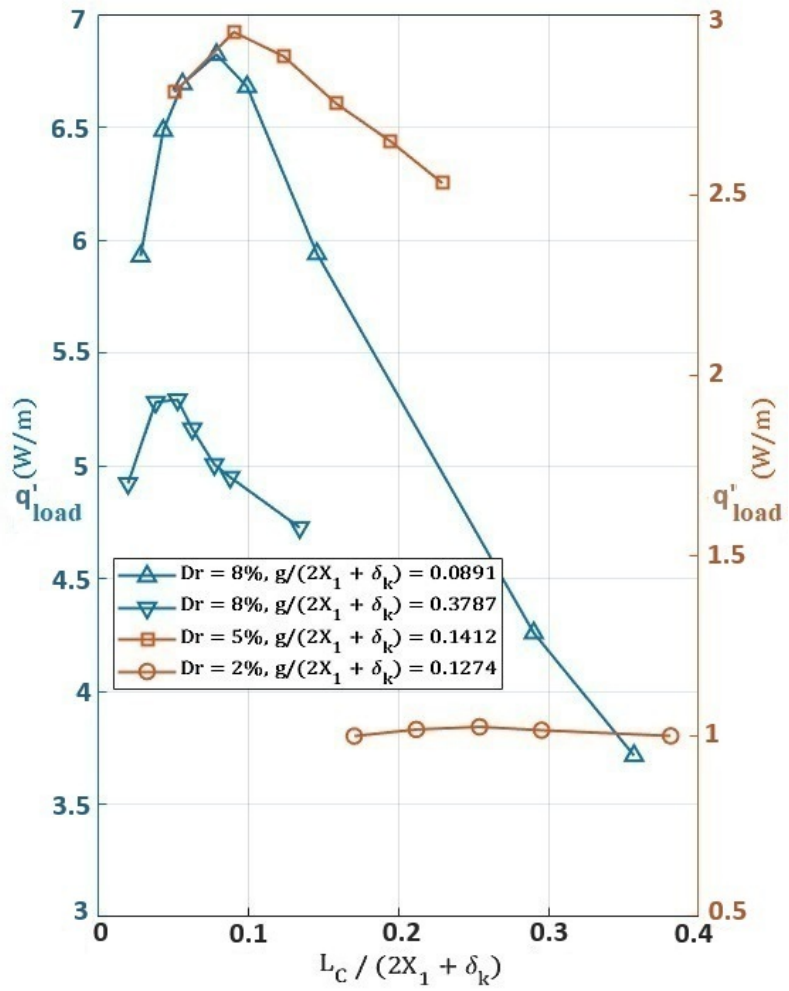

Figure 6: Variation of q'_{load} with L_c scaled with $(2X_1 + \delta_k)$. Curves are generated for different stack and g, and DR [94]. (Redrawn with permission).

the stack, which is controlled by particle transport. As a result, the cooling load decreases as the distance widens, due to the reduction in thermal coupling between the stack and the HXs. Similar results were mentioned by Besnion and Knio [94], as can be seen in Figure 7, where an optimum value of g is visible, and a lower or higher value decreases the q'_{load} for the CHX.

From the discussion of this Subsection, it is evident that initially when L was considered alone, a lot of discrepancies were found among the results. Further, by considering the ratio between the L and the X_1 along with the g, coherence between the different investigations was found. Later, it was further found that DR could be a deciding factor for the peak of q'_{load}. Therefore, it is recommended that for HX, at least L and g should be optimized

simultaneously, and the DR may suggest the optimal combination.

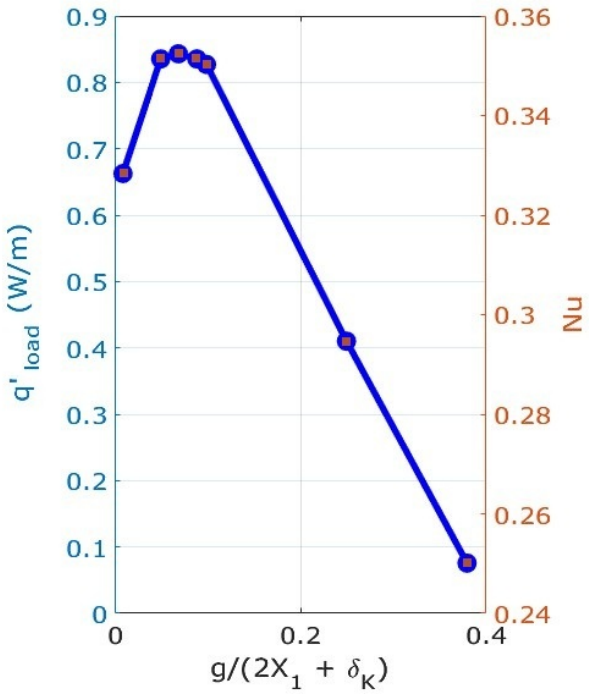

Figure 7: q'_{load} and Nu of CHX at various g scaled by $(2X_1 + \delta_k)$ [94]. (Redrawn with permission).

5.2 Effect of porosity (Φ)

The complicated turbulent flow patterns are thought to be caused by the difference in Φ [98]. Tijani et al. [41] suggested that to avoid abrupt flow entrance effects, the HX and stack should have matching Φ. This recommendation is based on the assumption that equal Φ allow the gas to flow without significant disturbances.

Besides, the Φ of the HX is related to the viscous dissipation and dissipation of acoustic power. Piccolo and Jaworski [78] conducted research with two different HXs having a Φ of 54% (A_{HX1}) and 33% (A_{HX2}). The authors found that A_{HX1}, having the higher Φ, had 23% more efficiency (calculated using a simplified 1D heat transfer model). The lower performance of A_{HX2} is associated with some less known acoustic loss mechanisms. One reason for this behavior could be the higher viscous dissipation in A_{HX2}. Indeed, the local V in A_{HX2} for a given volumetric flow should be approximately $\frac{\phi_1}{\phi_2}$, or 1.64 times greater than the velocity amplitude in A_{HX1}. Thus, for A_{HX2}, the viscous dissipation per unit area should be approximately $\left(\frac{\phi_1}{\phi_2}\right)^2 = 3.28$ times greater than that of A_{HX1}. A_{HX2}'s surface area $\left(\frac{\phi_2 R_{h1}}{\phi_1 R_{h2}}\right)$ is approximately 0.61 times smaller than A_{HX1}, meaning that A_{HX2}'s acoustic power dissipation is nearly twice that of A_{HX1}. Furthermore, Matveev et al. [99] mentioned the same, that

higher Φ minimizes the eddy production in acoustic flow. In addition, the dissipation of acoustic power is defined as $A_g \rho_m V^3$ [100], therefore, increasing V, increases the overall acoustic power loss.

Therefore, it can be concluded from these studies that when the HX is situated in high-velocity areas of the acoustic field, its comparatively small pore geometry, and Φ might have a significant impact on flow losses. Nevertheless, Ntimane and Tartibe [101] suggested that the performance of a TW TAE would be improved by considering a relatively shorter CHX having larger pores. However, the proper reason behind it could not be understood properly; therefore, further research is necessary to establish the fact or counter it.

Further, the inner spacing of the plates may exert a significant impact on the thermoviscous and heat transfer characteristics of the flow around the stack's edges, the HXs [29], and the region between these two elements [94]. The sudden variations in the sections and the multi-dimensional nonlinear mechanisms, including the production of harmonics, nonlinear thermal effects, and swirling jets, are controlled by the inner spacing, and g. Therefore, the inner spacing of the stack and the HX should be given proper consideration.

Belaid and Hireche [102] investigated four inner spacings (blockage ratio, β_r) for the HX to investigate the impact of it on the TA cooling performance by varying the thickness of the HXs. The authors also analyzed the effect of the g. The authors observed that the temperature around the CHX increases significantly when the β_r increases (Figure 8). This is not favorable for HX because, in order to have thermal pumping, the fluid temperature on the sides of the CHX needs to be lower than the solid temperature. The authors highlighted that the presence of turbulence increases the fluid's temperature. Therefore, the results of the study validated that a lower value of β_r reduces the dimensions and the effects of the vortex and gives a better refrigeration efficiency. However, in practice, it is quite difficult to fabricate stacks, and CHXs having a certain small β_r while maintaining the instructions for other parameters.

5.3 Effect of hydraulic radius (R_h)

The R_h offers valuable information about flow characteristics and facilitates the analysis of pressure drop and heat transfer efficiency. Lower pressure drops and better heat transfer efficiency are typically linked to an optimized R_h. Through numerical modeling of parallel plate stacks and HXs, Cao et al. [103] demonstrated the correlation between the L and R_h. This result suggests that the L of HXs with small pores ($R_h/\delta_k < 1$) may be shorter than $2X_1$, which is likewise the finding of another computational investigation [58]. However, for finned tube and plate HXs, the R_h also depends on the D (in addition to F_L), which is discussed in the following Subsection.

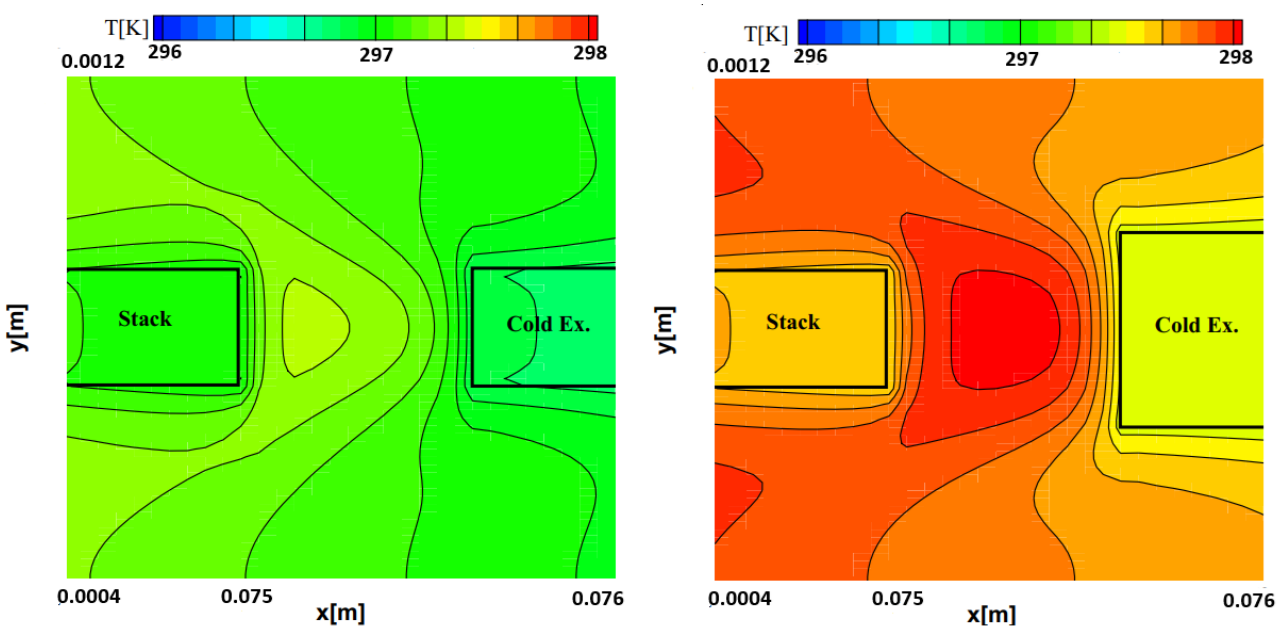

Figure 8: Temperature fields for the gap between the stack and the CHX at two different blockage ratios (left image β_r :1, and right image β_r: 3/2 [102]).(Reused with permission).

5.4 Effect of fin spacing (D or $2Yo$) or plate spacing (parallel plate HX)

The thermal performance of a TA system is significantly influenced by the plate spacing of HXs. Recent research published by Kamil et al. [104] concluded that the COP, coefficient of performance relative to Carnot (COPR), and efficiency of a TAR are highly dependent on the HXs. The results of the study are shown in Figure 9. At a specific ratio of plate spacing to thermal penetration depth (D/δ_k), the TAR operates at its best because the gas and the HX plates are in perfect thermal contact. It is evident from Figure 9 (a) that the D/δ_k values needed to achieve optimal cooling power fall within a range of values between 5 and 7.5. However, as the distance between the plates grows, the COP and COPR values also increase (refer to Figure 9 (b)). Considering both cooling power and thermal/overall performance, the optimal value D/δ_k is equal to 7, based on the data displayed in Figure 9 (a and b) from reference [104].

Further, to study the effect of D, Kamsanam et al. [29] designed three finned tube HXs with fin spacings of 0.7 mm, 1.4 mm, and 2.1 mm, respectively. The authors found that the value of the oscillating Nu increases with the increase of D. Similar findings were highlighted by Besnoin and Knio [94], where both the power density, q'_{load}, and consequently the heat transfer coefficient, increased with D. Piccolo and Pistone [105] reported that, for a given oscillation amplitude of the flow, the heat transfer surface area rapidly increases with D/δ_k when $D/\delta_k < 2.0$. The heat exchange length increases until D/δ_k is approximately 5.0; beyond this point, there is minimal change in the heat exchange length. Therefore, when

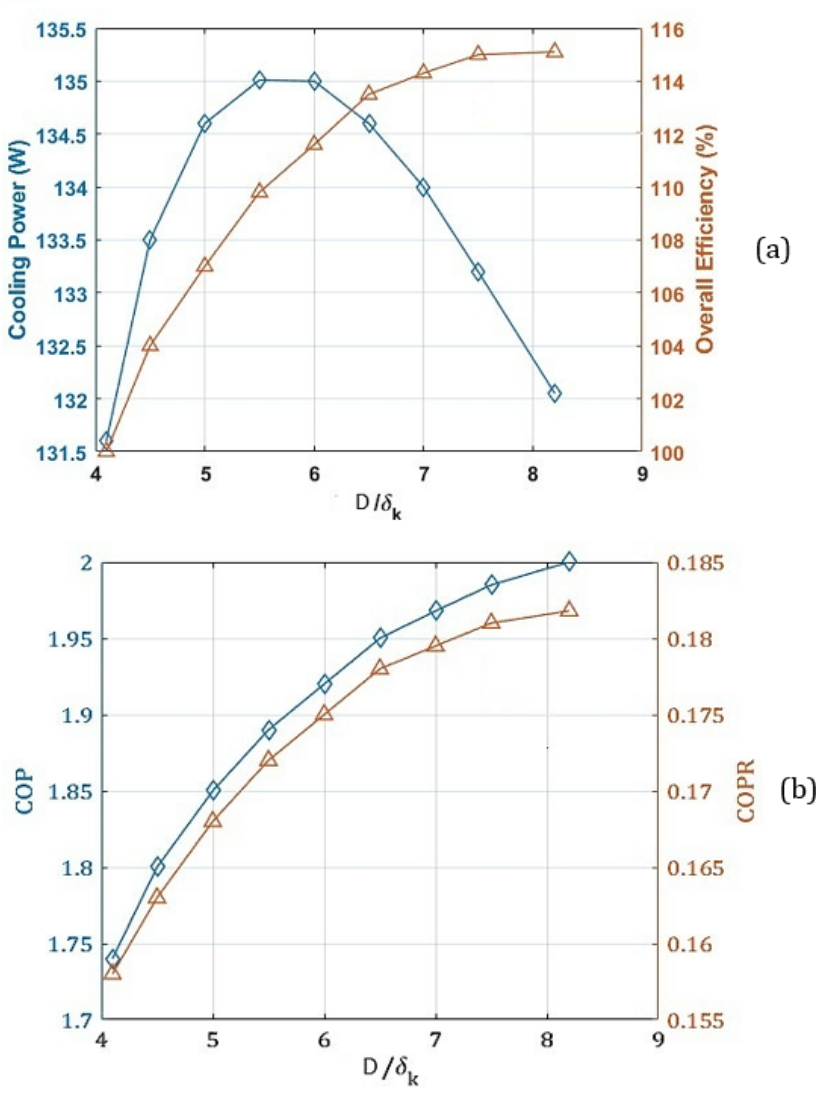

Figure 9: The effect of D/δ_k of HX on (a) cooling power, and overall efficiency and (b) COP, and COPR [104]. (Redrawn with permission).

the D is slightly increased (comparatively), it eventually increases Φ, resulting in reduced blockage and less effect of nonlinearities. However, a different set of results was reported by [86], where the authors observed that increasing the Φ beyond a certain limit leads to a decrease in performance. This apparent contradiction may stem from differences in the experimental setup. In [86], the stack was positioned between two HXs, whereas in [29], the two HXs were placed side by side. This difference in experimental procedure influences the flow dynamics and heat transfer characteristics.

Based on the discussion in Section 5, it is evident that, apart from the g, there is significant inconsistency among researchers regarding other parameters such as L, Φ, and D. This variability primarily arises from differences in the methods of analysis. Also, given the

complexity of the system, focusing on individual parameters for design optimization proves to be inadequate. The discrepancies observed in the literature stem from the simultaneous analysis of only a few parameters. Therefore, it is recommended that when evaluating HX, its L, g, Φ, and D should be optimized concurrently, considering both maximum heat transfer efficiency and minimum viscous dissipation.

6 Challenges

This Section addresses the general challenges associated with TA HXs. Unlike Sections 3, 4, and 5 - which provide in depth technical analyses along with specific recommendations on design, methodology, and analysis. This Section focuses on broader issues such as manufacturing, turbulence, and numerical studies. Recommendations are offered both for addressing these challenges and for guiding future research.

An optimal HX should minimize pressure drop and acoustic power loss while ensuring effective heat transfer. However, achieving this balance is challenging, yet to address these challenges, this Section is divided into three Subsections. First, fabrication challenges are discussed, highlighting fundamental manufacturing constraints and possible solutions. Next, turbulence measurement and treatment are examined as turbulence significantly affects HX efficiency and acoustic performance. Finally, the challenges of conducting numerical studies are explored, along with recommendations for improving simulation accuracy and reliability.

6.1 Fabrication challenges

There are fundamentally two major fabrication challenges while designing a HX for TA devices: pressure endurance, and the ratio of hydraulic radius to thermal penetration depth (R_h/δ_k). Besides, among other challenges, maintaining optimum dimension of F_L and Φ of HX are considerable.

It requires careful consideration to ensure that the HX can withstand a high pressure difference. Through the separation walls, cross-flow HXs experience a pressure difference between the increased mean pressure inside and the nearly ambient pressure outside. This pressure difference raises the possibility of wall rupture. Further, as metals lose strength at high temperatures and can no longer endure high pressure, designing the HHX presents a significant challenge.

Another parameter that determines the HX's performance is the ratio of the R_h to the δ_k. Arnott et al. [106] have declared that all the gas molecules participate in heat transfer at a ratio close to unity. Moreover, according to [45], increasing the mean pressure enhances the heat transfer of the HXs; however, as the mean pressure rises, δ_k decreases. When δ_k for a given gas at a given working frequency decreases, the R_h/δ_k ratio deviates from the

desired range (1 to 2); based on Arnott and Rott's analyses [106], keeping this ratio close to 1 is challenging as R_h would be very small.

Furthermore, another design problem is the low Φ of cross-flow HXs. Low Φ raises the velocity and displacement amplitude inside the HXs, which in some cases can be an advantage when adjusting the L to the particle displacement ratio; however, may increase viscous losses. As a result, the HX's overall pressure drops, and acoustic power loss increases [100]. Low Φ constrains the cross-sectional area of the channel, sometimes restricting both the gas to metal contact area and the heat transfer capacity of the HX. Small gas to solid contacts necessitate increasing the L in the direction of the oscillatory flow, which eventually increases pressure drop and acoustic power loss. Therefore, it is necessary to adjust Φ; however, fabricating a HX with very high Φ yet having enough heat transfer surface area is difficult.

Nevertheless, many of the above mentioned design restrictions imposed on potential HX forms can be overcome by using metal additive printing, a relatively new manufacturing technique that works layer by layer to form the entire part [107]. Hamood et al. [107] manufactured and tested three sets of HXs for TA systems using aluminum and stainless steel (Figure 10). Moreover, Wang et al. [108] mentioned that Inconel is an outstanding material for laser based additive manufacturing, though its adaptability for TA HX is a matter of concern. Further, to address the issue of poor thermal contact and gas leakage in traditional SW TAEs, Chen et al [109] fabricated an integrated stack using a "bottom up" layer by layer approach with the assistance of additive manufacturing. This study proved the feasibility and dependability of employing additive manufacturing for TA energy conversion, showing additive manufacturing's significant potential as a vital tool for future research. Therefore, it is recommended to use an additive manufacturing process wherever the geometry is complex.

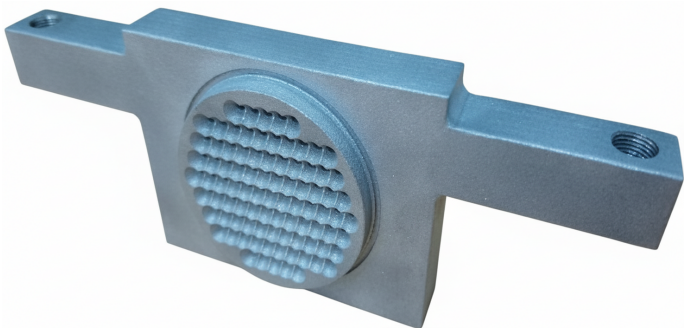

Figure 10: HX made by additive manufacturing [107].(Reused with permission).

6.2 Turbulence

In TA, to date, the effects of turbulence are not fully understood, as mentioned in Subsection 5.2. The performance of HXs largely depends on the turbulence and the eddy formation. Ideally, laminar flow across the HX would enable predictable heat transfer; in practice, turbulence promotes thermal diffusion, which, depending on the scale and structure of the turbulence, can either increase or decrease the system's performance. In some cases, small-scale turbulence close to HX can amplify the convective heat transfer; however, excessive turbulence can disrupt the phase relationship between temperature and pressure oscillations and increase viscous losses.

According to literature, solving the Navier-Stokes equations directly, or introducing a turbulence model are two viable methods to address the impacts of turbulence. Nevertheless, some researchers suggested that one can replicate the transitory effects of turbulence without the need for an additional model by utilizing high-fidelity numerical schemes, particularly if they are three dimensional [110] [111]. Similar to this, another method that has been employed in the literature is the employment of a laminar model in commercial programs with fine meshes and time steps, because these try to solve the macroscale and such models behave similarly to a Large eddy simulation (LES). On the other hand, these models do not employ any sub-grid model, which enables the numerical diffusion to dissipate even the smallest turbulent vortices [112] [113]. Nevertheless, no solid experimental data indicating the most appropriate turbulence model for TA are found in the literature. Although the k-ω SST turbulence model is the most widely used RANS model and provides comparatively better results [114][85][115], the best turbulence model for a genuine TA device should be assessed. Nevertheless, very recently Abdelmaged et al. [116] experimentally confirmed that a transition from laminar to a different regime occurs at a Re of 240 to 272 (here, Re is defined using the velocity amplitude and δ_v). To determine the critical Re (the Re at which flow changes), velocity fluctuations and Reynolds stress were estimated. At a Re of 272, an increase in Reynolds stress was observed at the boundary of the viscous penetration depth, indicating a shift in the flow regime. Though this experiment was conducted in an empty duct, but could be used as a ground for understanding. Besides, Ramadan et al. [117] investigated the characteristics of oscillating flow velocity field at the exit of different mesh grid regenerators, where a critical Re of 50 was determined, after which the flow becomes highly dissipative. Nevertheless, more experimental research should be conducted to determine when the laminar to turbulent transition occurs because turbulence favors heat transfer while increasing acoustic losses. It is of primary importance to progress on this understanding for a better design of HX.

6.3 Challenges with numerical study

We have software capable of modeling the operation of entire machines, but these tools rely on simplified descriptions of individual components, particularly HXs. Conversely, there are codes that can capture the detailed behavior within a HX, yet they fail to converge when applied to a full machine due to the wide range of time and spatial scales involved. The challenge in numerical studies is to bridge this gap.

There are some recognized design models available in literature for TA devices, such as DeltaEC [90], SAGE [118], PC-TAS [119]. The most widely used design tools are DeltaEC, developed by Los Alamos National Laboratory, and SAGE, developed by David Gedeon, though both are performance oriented and only partly discuss HX. Further, these codes are fundamentally different from each other, with DeltaEC using integration of the wave equation and SAGE using the finite difference method. SAGE is classified as a third-order, nodal analysis tool, while DeltaEC employs a similar one-dimensional approach that, to some extent, incorporates third-order characteristics [120]. In DeltaEC, several HX types are modeled based on gas flow geometry: parallel plate, TX (tubular), SX (screen), PX (porous), and variable exchangers VXT1, VXT2, VXQ1, and VXQ2. The parallel plate, and TX are smooth and short, SX and PX are porous and tortuous, while the VX models account for variable temperature and heat density along their length [121]. The DeltaEC HX model requires the user to adjust the solid temperature of the HX to get the heat flux or vice versa, besides providing the dimensions of A_g, L, and Φ. In SAGE, a more generalized object-oriented interface is used. SAGE can model matrix type heat exchangers (i.e. woven screen, random fiber, packed sphere, etc.,), tubular HX, fin HX etc. by connecting solid to fluid components, facilitating the prediction of axial temperature distribution [118] [122]. SAGE also employs semi-empirical terms for the friction factor, Nusselt number, and axial conductivity ratio. The use of few of these HXs such as fin type, parallel plates, etc. are seen in the literature and discussed in Table 2, and Figure 2. Further, smooth, short parallel plate, and TX models are straightforward, numerically stable, though they may oversimplify real geometries. SX and PX exchangers enhance heat transfer through increased surface area but involve additional parameters and can be sensitive to user input. SAGE HXs offer flexible modeling of complex geometries and solid–fluid interactions; however, reliance on semi-empirical correlations may limit accuracy. A direct distinction of these software from CFD is how it treats geometry and transport phenomena. CFD is capable of solving the governing equations on a mesh conforming to the actual geometry or close to the actual geometry [123], providing output of local heat and fluid flow. Complex flow patterns like secondary flows, vortices, and flow reversal can be captured using CFD, in contrast to the more straightforward methods of DeltaEC and SAGE. Nevertheless, this high-fidelity insight may come at a significantly higher computational cost (compared to DeltaEC and SAGE).

Yet after years of development, the TA phenomenon is difficult to describe with numerical calculations, as length scales that vary from a few millimeters inside the HXs to an order of meters inside the resonator. Furthermore, it is exceedingly challenging to evaluate the coupled nonlinear impacts of parameters on each other because the parameters that are crucial to the performance assessment of these devices are highly nonlinear and strongly dependent on one another. Therefore, the computational cost of the numerical algorithms required to assess these effects is very high. For example, transient simulations typically require time steps between 1.0×10^{-5} and 2.5×10^{-5} seconds [124] [125]. As a result, it is the main obstacle to the full simulation of complex systems and has mainly prevented further research from going beyond two dimensional models [126]. However, macroscopic domain simulations using commercial software could be a solution to full device simulation as for example, can be seen in Table 4. Macroscopic domain simulations using ANSYS Fluent and CFX are recommended for comprehensive device analysis based on literature results.

Table 4: Full device simulation - commercial software.

Reference of article	**Considered Parameters**	**Turbulence Model**	**Software with reference**
[127]	C_{fd}, C_{sf}, R_h, and Φ	Laminar	ANSYS-CFX [128]
[129]	Φ, β, and C	$K-\varepsilon$	ANSYS-Fluent [128]
[130]	Φ, β, and C	(LES	COMSOL Multiphysics [131]
[132]	Φ, β, and C	$K-\varepsilon$	ANSYS-Fluent
[133]	Φ, β, C and F_e	Lattice Boltzmann Method (LBM)	D2Q9 (mesh generation) [134]
[114]	Φ, β, and C	$K-\omega$	-
[85]	Φ, β, and C	$K-\omega$	ANSYS-Fluent
[115]	Φ, β, and C	$K-\omega$	ANSYS-Fluent

Here C_{fd} - coefficient of drag, C_{sf} - coefficient of skin friction, β - viscous resistance factor, C - nonlinear inertia resistance factor, and F_e - Forchheimer number.

7 Similitude study for future research

Considering the above discussion, it can be concluded that variations in operating parameters (mean pressure, frequency, working fluid, mean temperatures) and geometrical characteristics (even for HX of the same configuration) have a significant impact on heat transfer in

oscillatory flow. Besides, a lot of discrepancies are visible in the approaches leading to a lot of complexities in the design and analysis. Therefore, it is necessary to order a map for the design and analysis of HX for TA systems. As a result, a dimensional analysis and similitude can be a useful tool for examining and forecasting the behavior of the complex system. By using the concepts of spatial homogeneity and similarity, these techniques make physical issues easier to understand and handle through modeling, analysis, and experimentation. The system can be made simpler by using simplification to find the essential dimensionless parameters that control the system's behavior. Without having to cope with the complexities of the complete system, this simplification facilitates an easier understanding of the underlying physical events and favors applicability of results to other configurations.

For conducting dimensional analysis, two commonly used methods are Rayleigh's method and the Buckingham Pi theorem. Rayleigh's method is efficient when dealing with a small number of variables. However, since the TA HX involves many variables, the Buckingham Pi theorem is chosen for this study. The process begins by identifying all relevant variables and determining their fundamental dimensions. The number of dimensionless groups, known as π groups, is then calculated as the difference between the total number of variables and the number of fundamental dimensions. These π groups are formed by selecting suitable repeating variables that include all essential dimensions, simplifying the problem into a dimensionless form.

As mentioned, the first step is to define and classify all the variables needed to define the physics of the system considered, such as dimensions, gas properties, solid properties, other independent, and dependent variables.

To begin with, all the geometric dimensions that define the TA HX are considered based on Figure 4. Here, those are listed as A, R_h, F_L or L, F_T, D, Φ, The blockage ratio has not been considered here as it is inversely proportional to Φ.

For the calculation of gas, one fundamental assumption is taken into account: the fluid is an ideal gas. Here, T_{ref} is defined as a reference temperature at a constant temperature location in the HX (especially the CHX). Hereinafter, any variable defined with 'ref' as a subscript is evaluated at this constant T_{ref}. This assumption is made to evaluate the temperature-dependent variables. While running experiments, this T_{ref} can be adjusted according to the needs of the analysis. Besides pressure, there are fundamentally four parameters needed to specify an ideal gas: those are γ, a, K, and μ, which are the ratio of isobaric to isochoric specific heat, the speed of sound in the medium, thermal conductivity, and dynamic viscosity. Here, two extremely important parameters of gas density ρ and specific heat C_p are not separately considered as they are already incorporated in γ.

$$\gamma = \frac{C_p}{C_v}. \tag{25}$$

$$\rho = \frac{\gamma P}{a^2}. \tag{26}$$

Moreover, from the ideal gas consideration, the below relationships are originated. For an ideal gas, based on kinetic theory, the value of $q = w = 0.5$ (Equations 28 and 29). However, for noble gases that are used in TA, such as argon, helium, etc., this value changes. Therefore, for noble gases, the values of q and w should be determined. Nevertheless, under the ideal gas assumption, the determination of q and w is neglected in this calculation.

$$a(T) = a_{\text{ref}} \left(\frac{T}{T_{\text{ref}}} \right)^{0.5}. \tag{27}$$

$$K(T) = K_{\text{ref}} \left(\frac{T}{T_{\text{ref}}} \right)^{q}. \tag{28}$$

$$\mu(T) = \mu_{\text{ref}} \left(\frac{T}{T_{\text{ref}}} \right)^{w}. \tag{29}$$

The properties of the solids include the material, K_s and $\rho_s C_s$. The other miscellaneous independent variables are referred to here as Sundry variables. For a TA HX, the variables are $\dot{Q}_{\text{load}}$, P_m, T_{ref}, and f. The pressure is defined as Equation 30, where $P(t)$ is a 1st order acoustic term. Similarly, other variables such as temperature also possess a mean and a fluctuating part.

$$P = P_m + P(t). \tag{30}$$

Now, the dependent variables are those variables that depend on the above mentioned independent variables. The independent variables can be adjusted when designing the experiments, but dependents are nonadjustable directly. The fundamental dependent variables are temperature $T(x,t)$, velocity $V(x,t)$, pressure $P(x,t)$, effectiveness ε, and efficiency η. Among these, ε, and η are already dimensionless.

To summarize, all the considered list of variables are:

- Geometry: A, R_h, L (or F_L), F_T, D, Φ
- Gas: γ, a_{ref}, K_{ref}, μ_{ref}, q, w
- Solid: K_s, $\rho_s C_s$
- Sundry: $\dot{Q}_{\text{load}}$, P_m, T_{ref}, f
- Dependent: $T(x,t)$, $V(x,t)$, $P(x,t)$, ε, η

A clear understanding will provide us with four fundamental variables: length, temperature, time, and mass. Considering this, the repeating variables are taken as L, P_m, a_{ref}, and T_{ref}. All the other variables are normalized using the repeating variables and the results are:

- Geometry: $\frac{A}{L^2}$, $\frac{R_h}{L}$, $\frac{X_i}{L}$ (where index i refers to the fin geometrical parameters, as they all can be normalized by L)
- Gas: γ, $\frac{K_{\text{ref}}T_{\text{ref}}}{a_{\text{ref}}P_mL}$, $\frac{\mu_{\text{ref}}a_{\text{ref}}}{P_mL}$, q, w
- Solid: $\frac{K_sT_{\text{ref}}}{a_{\text{ref}}P_mL}$, $\frac{\rho_sC_sT_{\text{ref}}}{P_m}$
- Sundry: $\frac{\dot{Q}_{\text{load}}}{P_ma_{\text{ref}}L^2}$, $\frac{a_{\text{ref}}}{fL}$
- Dependent: $\frac{T(x,t)}{T_{\text{ref}}}$, $\frac{V(x,t)}{a_{\text{ref}}}$, $\frac{P(x,t)}{P_m}$, ε, η

For more clarity, some adjustments are made. For instance, $\frac{\mu_{\text{ref}}a_{\text{ref}}}{P_mL}$ is replaced with the Pr, which can be written as $\frac{\mu C_p}{K}$. This replacement is done because both are dimensionless and represent the same property of the gas. Further, the cooling load $\frac{\dot{Q}_{\text{load}}}{P_ma_{\text{ref}}L^2}$ is theoretically debatable to be defined by the cross-sectional area of the HX instead of its length. However, we will keep it normalized with L as most current research defines the property $\dot{Q}_{\text{load}}$ with L. Finally, we replace $\frac{K_{\text{ref}}T_{\text{ref}}}{a_{\text{ref}}P_mL}$ with the more relevant thermal penetration depth term of TA systems, likely $\frac{\delta_k}{R_h}$, where $\delta_k = \sqrt{\frac{K_{\text{ref}}}{\pi f \rho_{\text{ref}} c_p}}$ (density and specific heat are considered in γ). Density, which is incorporated in γ, can be normalized as $\frac{\rho_{\text{ref}}a_{\text{ref}}L}{\mu_{\text{ref}}}$, which is usually referred to as the Re. The term L can be replaced with the more sophisticated term $\delta_v = \sqrt{\frac{2\mu_{\text{ref}}}{2\pi f \rho_{\text{ref}}}}$ (viscous penetration depth) as suggested by [45]. Thus, for the HX of a TA system, where S_t is the Strouhal number (ratio of inertial forces due to unsteady periodic velocities to inertia forces due to changes in steady flow):

$$\begin{bmatrix} \frac{T(x,t)}{T_{\text{ref}}} \\ \frac{P(x,t)}{P_{\text{ref}}} \\ \frac{V(x,t)}{a_{\text{ref}}} \\ \epsilon \\ \eta \end{bmatrix} = g \begin{bmatrix} \frac{A_{\text{ref}}}{L^2} & \frac{R_h}{L} & \frac{X_i}{L} \\ \gamma & Pr & \frac{\delta_k}{R_h} \\ \frac{K_sT_{\text{ref}}}{a_{\text{ref}}P_mL} & \frac{\rho_sC_sT_{\text{ref}}}{P_m} & Re \\ \frac{\dot{Q}_{\text{load}}}{P_ma_{\text{ref}}L^2} & St & \end{bmatrix}. \tag{31}$$

The principle of similitude recommends keeping the dimensionless independent variables on the right side and the dependents on the left, that's what has been done in the above Equation 31. A clear observation shows that by grouping the variables and normalizing them using the repeating variable, we have reduced nearly half of the relevant parameters. This results in a significant reduction in the number of experiments required compared to previous approaches. The list of non-dimensional numbers identified in Equation 31 should be considered when analyzing TA HXs, although in most literature, only a few of these are typically taken into account. Moreover, dimensional analysis of the fundamental equations (continuity, momentum, and energy) shows that the considered 24 variables are sufficient for the dimensional analysis of TA HX.

From the above discussion and literature review, it is noticeable that a modification in the regression variables of $Nu = Nu\,(Re, Pr)$ is necessary. In the conventional Nu equations, Re

provides the flow pattern considering inertial and viscous forces, and Pr defines momentum and thermal diffusivity. However, in acoustically oscillating flow, the flow characteristics differ from conventional fluid flow as the particles move back and forth in a periodic motion. Therefore, based on the similitude study, it is recommended to reconsider the formation of the regression analysis and to include the acoustic frequency by incorporating the Strouhal number (St). The recommended correlation formation is therefore:

$$Nu = Nu\left(Re, Pr, St\right). \tag{32}$$

In the Equation 32, the characteristic length scale of the Re can be the velocity amplitude and the hydraulic diameter. Whereas, in the St, the common choice can be plate spacing or D or R_h (needs to be defined by experiment). Besides, the set of Equations in 31 needs to be considered for proper analysis and optimization.

8 Conclusion

This review provides a thorough evaluation of HXs in TA systems, addressing their configurations, performance parameters, key geometrical considerations, design criteria and methodologies, limitations, and prospects. The study synthesizes research from various sources, spanning both experimental and numerical approaches and ranging from studies on isolated solid plates to entire HXs and full TA devices. The review covers a broad range of viewpoints, including the performance of the device, heat transfer, entropy generation, and practical design issues. It also delves into design limitations and provides strategies for overcoming these challenges. By integrating studies of different natures, the review not only highlights critical insights from various research perspectives but also identifies the gaps and challenges that remain in optimizing TA HX design. Based on the extensive discussion, the key conclusions are summarized below.

- Currently, there is no well defined methodology for designing HXs for TA systems. Many of the existing design criteria and methodologies are directly adopted from steady flow applications, which do not fully account for the unique flow patterns and dynamics of oscillating flow. Given the significant differences between steady and oscillating flow regimes, further research is essential to develop a comprehensive and optimized design methodology tailored to TA HXs.
- Given the complexity of the system, focusing on individual parameters for design optimization proves to be inadequate. The discrepancies observed in the literature stem from the analysis of only a few parameters. Therefore, it is recommended that when evaluating HX, at a minimum, its L, g, Φ, and D should be optimized concurrently along with varying DR, considering both maximum heat transfer and minimum viscous

dissipation. Ideally, the set of similitude parameters determined in Section 7 should be considered.

- Different types of HXs have been discussed in the literature. However, based on some recent studies, it appears that finned tube HXs are comparatively more studied than other types of HXs. However, more constructive research should be conducted on their performance and optimization, specially on F_L and F_T, and g. Additionally, additive fabrication may be considered depending on their geometrical complexity.
- The steady heat transfer models are not fully applicable to oscillating flow. For laminar regime, the adopted steady models significantly underestimate the heat transfer. Further, the developed correlations for oscillating flow are also system specific. Therefore, this study has organized all available oscillating flow correlations according to the Re and suggests a new form of regression correlation for consideration in future research to better understand and evaluate the heat transfer processes.
- So far, no proper method has been developed for analyzing the ε of TA HXs. The problem generally lies in the measurement of the property $\dot{Q}_{\text{load}}$. Therefore, further research is necessary to establish a proper experimental method to quantify this properly.
- One of the major challenges of oscillating flow is turbulence. The behavior of turbulence and its effects on HX are not yet properly understood. Therefore, further research is necessary to understand the phenomena and optimize HX design to minimize its adverse effects. Advancing in numerical methods can help in understanding the phenomena and optimizing the design.
- In this study, a similitude study has been conducted, which identifies fundamental parameters for better optimization and analysis. This simplification facilitates an easier understanding of the underlying physical events without having to cope with the complexities of the complete system.

Several paths for future research were drawn in this paper. The main ones are: future studies should optimize TA HXs by considering all key design parameters collectively and using the Equations in 31 to reduce the number of experiments and variables, with convective heat transfer evaluated via Equation 32. The determination of $\dot{Q}_{load}$ requires further research, accounting for oscillatory flow, turbulence, end effects, and laminar to turbulent transition. While the k-ω SST turbulence model is more accurate than other RANS models, custom numerical models may improve predictions. Finally, different HXs and additive manufacturing with aluminum alloys should be explored for superior heat transfer in complex geometries.

References

[1] John William Strutt Baron Rayleigh. The theory of sound. *Elsevier*, 2, 1896.

[2] Lei Xiao, Kaiqi Luo, Zhanghua Wu, Jiaxin Chi, Jingyuan Xu, Limin Zhang, Jianying Hu, and Ercang Luo. A highly efficient heat-driven thermoacoustic cooling system. *Cell Reports Physical Science*, 5(2), 2024.

[3] Michael AG Timmer, Kees de Blok, and Theo H van der Meer. Review on the conversion of thermoacoustic power into electricity. *The Journal of the Acoustical Society of America*, 143(2):841–857, 2018.

[4] Kai Wang, Seth R Sanders, Swapnil Dubey, Fook Hoong Choo, and Fei Duan. Stirling cycle engines for recovering low and moderate temperature heat: A review. *Renewable and Sustainable Energy Reviews*, 62:89–108, 2016.

[5] Tao Jin, Jiale Huang, Ye Feng, Rui Yang, Ke Tang, and Ray Radebaugh. Thermoacoustic prime movers and refrigerators: Thermally powered engines without moving components. *Energy*, 93:828–853, 2015.

[6] Praitoon Chaiwongsa and Somchai Wongwises. Experimental investigation on the performance of the air-based standing wave thermoacoustic refrigerator using heat pipe as heat exchangers. *International Journal of Air-Conditioning and Refrigeration*, 28(01):2050007, 2020.

[7] AR Irfan, MZM Zarhamdy, SM Sazli, HM Hafiz, and A Azlida. Analysis of hot heat exchangers performance of thermoacoustic energy converter. In *AIP Conference Proceedings*, volume 2030, page 020313. AIP Publishing LLC, 2018.

[8] Andrew W Avent and Chris R Bowen. Principles of thermoacoustic energy harvesting. *The European Physical Journal Special Topics*, 224(14):2967–2992, 2015.

[9] John Wheatley, T Hofler, Gregory William Swift, and Albert Migliori. Understanding some simple phenomena in thermoacoustics with applications to acoustical heat engines. *American journal of physics*, 53(2):147–162, 1985.

[10] Gregory William Swift. Thermoacoustic engines. *the Journal of the Acoustical Society of America*, 84(4):1145–1180, 1988.

[11] Antonio Piccolo. Numerical study of entropy generation within thermoacoustic heat exchangers with plane fins. *Entropy*, 17(12):8228–8239, 2015.

[12] Antonio Piccolo. Optimization of thermoacoustic refrigerators using second law analysis. *Applied energy*, 103:358–367, 2013.

[13] Nor Atiqah Zolpakar, Normah Mohd-Ghazali, and Mawahib Hassan El-Fawal. Performance analysis of the standing wave thermoacoustic refrigerator: A review. *Renewable and sustainable energy reviews*, 54:626–634, 2016.

[14] Ashish S Raut and Uday S Wankhede. Review of investigations in eco-friendly thermoacoustic refrigeration system. *Thermal Science*, 21(3):1335–1347, 2017.

[15] Prajwal C Bansod and Ashish S Raut. Review on thermoacoustic refrigeration. *International Journal of Innovations in Engineering and Science*, 2(3):18–24, 2017.

[16] LK Tartibu. Developing more efficient travelling-wave thermo-acoustic refrigerators: A review. *Sustainable Energy Technologies and Assessments*, 31:102–114, 2019.

[17] Geng Chen, Lihua Tang, Brian Mace, and Zhibin Yu. Multi-physics coupling in thermoacoustic devices: A review. *Renewable and Sustainable Energy Reviews*, 146:111170, 2021.

[18] Shahryar Zare, AR Tavakolpour-Saleh, A Aghahosseini, and Reza Mirshekari. Thermoacoustic stirling engines: A review. *International Journal of Green Energy*, 20(1):89–111, 2021.

[19] Ussama Ali, Omar Al-Mufti, and Isam Janajreh. Harnessing sound waves for sustainable energy: Advancements and challenges in thermoacoustic technology. *Energy Nexus*, 15:100320, 2024.

[20] Armando Di Meglio and Nicola Massarotti. Cfd modeling of thermoacoustic energy conversion: a review. *Energies*, 15(10):3806, 2022.

[21] Jiale Huang, Rui Yang, Yupeng Yang, Qiang Zhou, and Ercang Luo. Generalized thermoacoustic heat engines with unconventional working substances: A review. *Applied Energy*, 347:121447, 2023.

[22] Mahyar Fazli, Karim Mazaheri, Mohammad Ja'fari, Artur J Jaworski, and Abbas Babaei Zarch. Heat-driven thermoacoustic refrigeration: A comprehensive review of technologies, applications, trends and challenges. *Applied Thermal Engineering*, 260:124996, 2025.

[23] Mahesh Krishna Gaikwad, Savita Shinde, Abhijit L Dandavate, Mithul J Naidu, Tushar A Jadhav, Sachin Salunkhe, and Robert Čep. Advancements in thermoacoustic technology: a comprehensive review and analysis of recent research. *International Journal of Air-Conditioning and Refrigeration*, 33(1):14, 2025.

[24] Jing Wen, Lingxiao Zhang, Huifang Kang, Shuli Liu, and Kai Wang. Advances in the utilization and suppression of thermoacoustic effect: A review. *International Journal of Heat and Mass Transfer*, 231:125758, 2024.

[25] Mohammed Abed and Qais Abid Yousif. Design and manufacture of a thermo-acoustic refrigerator by applying high-amplitude sound waves to compress cooling agent: a review. *Journal of Thermal Analysis and Calorimetry*, pages 1–13, 2025.

[26] Antonio Piccolo, Roberto Siclari, Fabrizio Rando, and Mauro Cannistraro. Comparative performance of thermoacoustic heat exchangers with different pore geometries in oscillatory flow. implementation of experimental techniques. *Applied Sciences*, 7(8):784, 2017.

[27] Islam A Ramadan, Hélène Bailliet, Gaëlle Poignand, and David Gardner. Design, manufacturing and testing of a compact thermoacoustic refrigerator. *Applied Thermal Engineering*, 189:116705, 2021.

[28] Kaixin Wang and Zhan-Chao Hu. Experimental investigation of a novel standing-wave thermoacoustic engine based on pche and supercritical co2. *Energy*, 282:128334, 2023.

[29] Wasan Kamsanam, Xiaoan Mao, and Artur J Jaworski. Thermal performance of finned-tube thermoacoustic heat exchangers in oscillatory flow conditions. *International Journal of Thermal Sciences*, 101:169–180, 2016.

[30] Fatimah AZ Mohd Saat and Artur J Jaworski. Oscillatory flow and heat transfer within parallel-plate heat exchangers of thermoacoustic systems. In *Proceedings of the World Congress on Engineering 2013. Lecture Notes in Engineering and Computer Science*, volume 3, pages 1699–1704. Newswood Limited, 2013.

[31] Kriengkrai Assawamartbunlue and Channarong Wantha. Oscillating heat transfer correlations for spiral-coil thermoacoustic heat exchangers. *Journal of Thermal Science and Engineering Applications*, 7(3):031008, 2015.

[32] Martin Wetzel and Cila Herman. Design optimization of thermoacoustic refrigerators. *International journal of refrigeration*, 20(1):3–21, 1997.

[33] H Ishikawa and PA Hobson. Optimisation of heat exchanger design in a thermoacoustic engine using a second law analysis. *International Communications in Heat and Mass Transfer*, 23(3):325–334, 1996.

[34] G Alefeld. What are thermodynamic losses and how to measure them. In *A Future for Energy, Proceedings of the World Energy Symposium*, 1990.

[35] RA Hiller and Gregory William Swift. Condensation in a steady-flow thermoacoustic refrigerator. *The Journal of the Acoustical Society of America*, 108(4):1521–1527, 2000.

[36] Nathan Blanc, Michael Laufer, Steven Frankel, and Guy Z Ramon. High-fidelity numerical simulations of a standing-wave thermoacoustic engine. *Applied Energy*, 360:122817, 2024.

[37] Mahmut Reyhanoglu and Mohammad Jafari. Learning-enabled robust control of thermoacoustic oscillations. *Electronics*, 14(9):1771, 2025.

[38] Martin Wetzel and Cila Herman. Experimental study of thermoacoustic effects on a single plate part i: Temperature fields. *Heat and mass transfer*, 36(1):7–20, 2000.

[39] Yaoyu Li, Brian L Minner, George T-C Chiu, Luc Mongeau, and James E Braun. Adaptive tuning of an electrodynamically driven thermoacoustic cooler. *The Journal of the Acoustical Society of America*, 111(3):1251–1258, 2002.

[40] MEH Tijani, JCH Zeegers, and ATAM De Waele. Prandtl number and thermoacoustic refrigerators. *The Journal of the Acoustical Society of America*, 112(1):134–143, 2002.

[41] MEH Tijani, JCH Zeegers, and ATAM De Waele. Design of thermoacoustic refrigerators. *Cryogenics*, 42(1):49–57, 2002.

[42] Daniel A Russell and Pontus Weibull. Tabletop thermoacoustic refrigerator for demonstrations. *American Journal of Physics*, 70(12):1231–1233, 2002.

[43] David Marx and Philippe Blanc-Benon. Computation of the mean velocity field above a stack plate in a thermoacoustic refrigerator. *Comptes rendus. Mécanique*, 332(11):867–874, 2004.

[44] Fathi Jebali, Jean Valentin Lubiez, and Maurice-Xavier François. Response of a thermoacoustic refrigerator to the variation of the driving frequency and loading. *International journal of refrigeration*, 27(2):165–175, 2004.

[45] Emmanuel C Nsofor, Serdar Celik, and Xudong Wang. Experimental study on the heat transfer at the heat exchanger of the thermoacoustic refrigerating system. *Applied Thermal Engineering*, 27(14-15):2435–2442, 2007.

[46] Hadi Babaei and Kamran Siddiqui. Design optimization of parallel plate heat exchangers in thermoacoustic devices. *Canadian Acoustics*, 35(3):170–171, 2007.

[47] Normah M Ghazali, Prof Dr Azhar Abd Aziz, Srithar Rajoo, and Nor Aswadi Che Sidek. Environmentally friendly refrigeration with thermoacoustic. *Fakulti Kejuruteraan Mekanikal, Universiti Teknologi Malaysia. Research Vote*, (74166).

[48] MR Osorio, A Bétrancourt, MX François, JA Veira, and F Vidal. A superconducting fault current limiter integrated in the cold heat exchanger of a thermoacoustic refrigerator. *Superconductor Science and Technology*, 21(9):095013, 2008.

[49] Ph Blanc-Benon and A Berson. Nonlinear heat transport between the stack and the heat-exchangers of standing-wave thermoacoustic refrigerators. In *AIP Conference Proceedings*, volume 1022, pages 359–362. American Institute of Physics, 2008.

[50] Meghan Labounty and Andrew Lingenfelter. Design and construction of a thermoacoustic refrigerator. *Project PH GSI-0706, Worcester Polytechnic Institute, Apr*, 2008.

[51] N Mohd-Ghazali, CF Cheng, and S Nurudin. A malaysian portable thermoacoustic refrigerator system. In *Proceedings of the 13th Int. AMME Conference*, volume 27, page 29, 2008.

[52] Cila Herman, Christopher Lavin, and Trávníček Zdeněk. Performance of thermoacoustic refrigerators: cooling load and coefficient of performance. In *Heat Transfer Summer Conference*, volume 48494, pages 755–760, 2008.

[53] Emmanuel C Nsofor and Azrai Ali. Experimental study on the performance of the thermoacoustic refrigerating system. *Applied Thermal Engineering*, 29(13):2672–2679, 2009.

[54] Chao Shen, Yaling He, Yuguang Li, Hanbing Ke, Dongwei Zhang, and Yingwen Liu. Performance of solar powered thermoacoustic engine at different tilted angles. *Applied Thermal Engineering*, 29(13):2745–2756, 2009.

[55] MA Teamah, MM Dawood, and WM El-Maghlany. Thermoacoustic refrigeration in different gases for different frequencies. *Alexandria Engineering Journal*, 48(3):233–240, 2009.

[56] Lei Shi, Xiaoan Mao, and Artur J Jaworski. Application of planar laser-induced fluorescence measurement techniques to study the heat transfer characteristics of parallel-plate heat exchangers in thermoacoustic devices. *Measurement Science and Technology*, 21(11):115405, 2010.

[57] Xiaoan Mao, Lei Shi, Artur J Jaworski, and Wasan Kamsanam. Heat transfer on parallel plate heat exchangers in an oscillatory flow. In *Engineering Systems Design and Analysis*, volume 49163, pages 653–661, 2010.

[58] Antonio Piccolo. Numerical computation for parallel plate thermoacoustic heat exchangers in standing wave oscillatory flow. *International Journal of Heat and Mass Transfer*, 54(21-22):4518–4530, 2011.

[59] Dianpeng Zhao Fang Chen Xu, Jiangrong and Shanshan Xu. Numerical simulating for turbulent heat transfer of thermoacoustic cooler. *Procedia Engineering*, 16(789-795), 2011.

[60] MM Bassem, Y Ueda, and A Akisawa. Design and construction of a traveling wave thermoacoustic refrigerator. *International journal of refrigeration*, 34(4):1125–1131, 2011.

[61] A Ibrahim, Hosny Omar, and Ehab Abdel-Rahman. Constraints and challenges in the development of loudspeaker-driven thermoacoustic refrigerator. In *18th International Congress on Sound & Vibration, ICSV18, Rio de Janeiro, Brazil*, pages 10–14, 2011.

[62] Syeda Tasnim, Shohel Mahmud, and Roydon Fraser. Measurements of thermal field at the stack extremities of a standing wave thermoacoustic heat pump. *Frontiers in Heat and Mass Transfer (FHMT)*, 2(1), 2011.

[63] NM Arafa, AH Ibrahim, K Addas, and Ehab Abdel-Rahman. Design considerations for thermoacoustic engines for low onset temperature and efficient operation. In *Forum Acusticum*, volume 27, pages 961–966, 2011.

[64] XH Hao, YL Ju, Upendra Behera, and Srinivasan Kasthurirengan. Influence of working fluid on the performance of a standing-wave thermoacoustic prime mover. *Cryogenics*, 51(9):559–561, 2011.

[65] Artur J Jaworski and Antonio Piccolo. Heat transfer processes in parallel-plate heat exchangers of thermoacoustic devices–numerical and experimental approaches. *Applied Thermal Engineering*, 42:145–153, 2012.

[66] Na Pan, Chao Shen, and Shuangfeng Wang. Experimental study on the flow and heat transfer characteristics of thermoacoustic core. *Experimental thermal and fluid science*, 44:219–226, 2013.

[67] Wasan Kamsanam, Xiaoan Mao, and Artur J Jaworski. Development of experimental techniques for measurement of heat transfer rates in heat exchangers in oscillatory flows. *Experimental Thermal and Fluid Science*, 62:202–215, 2015.

[68] NM Hariharan, P Sivashanmugam, and S Kasthurirengan. Experimental investigation of a thermoacoustic refrigerator driven by a standing wave twin thermoacoustic prime mover. *International journal of refrigeration*, 36(8):2420–2425, 2013.

[69] Olusegun M Ilori, Xiaoan Mao, and Artur J Jaworski. Numerical simulation of oscillatory flow and heat transfer in the heat exchangers of thermoacoustic systems. In *Proceedings of ICR2015*. International Institute of Refrigeration, 2015.

[70] Mohamed Zouhir Dar Ramdane, Miloud Abidat, and Mohamed Hamel. Numerical simulation of heat exchanger's length's effect in a thermoacoustic engine. *Journal of Physical Science and Application*, 5:61–65, 2015.

[71] Mohammad Gholamrezaei and Kaveh Ghorbanian. Thermal analysis of shell-and-tube thermoacoustic heat exchangers. *Entropy*, 18(8):301, 2016.

[72] Fatimah AZ Mohd Saat and Artur J Jaworski. The effect of temperature field on low amplitude oscillatory flow within a parallel-plate heat exchanger in a standing wave thermoacoustic system. *Applied Sciences*, 7(4):417, 2017.

[73] Wasan Kamsanam. Effects of stack and heat exchanger configurations on thermal performance of a thermoacoustic refrigerator. *Naresuan University Engineering Journal*, 13(2):26–34, 2018.

[74] Olusegun M Ilori, Artur J Jaworski, and Xiaoan Mao. Experimental and numerical investigations of thermal characteristics of heat exchangers in oscillatory flow. *Applied Thermal Engineering*, 144:910–925, 2018.

[75] Antonio Piccolo, Alessio Sapienza, and Cecilia Guglielmino. Convection heat transfer coefficients in thermoacoustic heat exchangers: An experimental investigation. *Energies*, 12(23):4525, 2019.

[76] Jakub Kajurek, Artur Rusowicz, and Andrzej Grzebielec. Design and simulation of a small capacity thermoacoustic refrigerator. *SN Applied Sciences*, 1(6):579, 2019.

[77] Haoran Huang and Artur Jaworski. Numerical simulation of the effect of plate spacing on heat transfer characteristics within a parallel-plate heat exchanger in a standing wave thermoacoustic system. In *E3S Web of Conferences*, volume 116, page 00028. EDP Sciences, 2019.

[78] Antonio Piccolo and Artur J Jaworski. Experimental study of heat transfer characteristics of finned-tube and circular-pore heat exchangers in oscillatory flow. *Applied Thermal Engineering*, 181:116022, 2020.

[79] Chou Aw Lin, Fatimah Al Zahrah Mohd Saat, Fadhliah Shikh Anuar, Mohamad Firdaus Sukri, Mohd Zaid Akop, and Patcharin Saechan. The impact of working gas on heat transfer performance of tube banks heat exchanger in a thermoacoustic system. *International Journal of Nanoelectronics & Materials*, 15, 2022.

[80] Ahmed Hamood, Mohammad Ja'fari, and Artur J Jaworski. Synthetic jet flow driven by a standing-wave thermoacoustic heat engine. *Thermal Science and Engineering Progress*, 39:101725, 2023.

[81] Ariana Martinez, Mario Tindaro Migliorino, Carlo Scalo, and Stephen D Heister. Experimental and numerical investigation of standing-wave thermoacoustic instability under transcritical temperature conditions. *The Journal of the Acoustical Society of America*, 150(4):2900–2911, 2021.

[82] Karim Mazaheri and Mahyar Fazli. Exergy-based methodology to develop design guidelines for performance optimization of a coupled co-axial thermoacoustic refrigerator. *International Journal of Thermofluids*, 20:100451, 2023.

[83] Geng Chen, Kai Wang, Shancheng Tao, Long Gao, Zhaoyu Li, Jiawen Xu, and Lihua Tang. Experimental study on the cooling performances of thermoacoustic heat exchangers. *International Journal of Heat and Mass Transfer*, 241:126759, 2025.

[84] Insu Paek, James E Braun, and Luc Mongeau. Characterizing heat transfer coefficients for heat exchangers in standing wave thermoacoustic coolers. *The Journal of the Acoustical Society of America*, 118(4):2271–2280, 2005.

[85] Fatimah AZ Mohd Saat and Artur J Jaworski. Numerical predictions of early stage turbulence in oscillatory flow across parallel-plate heat exchangers of a thermoacoustic system. *Applied Sciences*, 7(7):673, 2017.

[86] MM Mahlalela, MGK Machesa, and LK Tartibu. Investigating the synergy of blockage ratio and external cold heat exchanger in standing-wave thermoacoustic engines: An experimental study. *Results in Engineering*, 23:102424, 2024.

[87] Cila Herman and Yuwen Chen. A simplified model of heat transfer in heat exchangers and stack plates of thermoacoustic refrigerators. *Heat and mass transfer*, 42(10):901–917, 2006.

[88] Junjiao Yang and Zhan-Chao Hu. Deep reinforcement learning for optimizing the thermoacoustic core in a supercritical co2 thermoacoustic engine. *Energy*, 325:135950, 2025.

[89] Gregory William Swift. Analysis and performance of a large thermoacoustic engine. *the Journal of the Acoustical Society of America*, 92(3):1551–1563, 1992.

[90] John P Clark, William C Ward, and Gregory William Swift. Design environment for low-amplitude thermoacoustic energy conversion (deltaec). *The Journal of the Acoustical Society of America*, 122(5_Supplement):3014–3014, 2007.

[91] Liang Zhou, Tieyu Gao, Yonghao Wang, Jiadian Wang, Jianying Gong, and Jun Li. Large eddy simulation of enhanced heat transfer in grooved channel with pulsating flow corresponding to hydrodynamic frequency. *International Journal of Heat and Mass Transfer*, 218:124822, 2024.

[92] K Tang, J Yu, T Jin, YP Wang, WT Tang, and ZH Gan. Heat transfer of laminar oscillating flow in finned heat exchanger of pulse tube refrigerator. *International Journal of Heat and Mass Transfer*, 70:811–818, 2014.

[93] Fatimah AZ Mohd Saat, Artur J Jaworski, and Ahmed Hamood. The effect of operating conditions on heat transfer for parallel plate heat exchangers of thermoacoustic standing wave systems. *International Journal of Thermofluids*, 23:100771, 2024.

[94] Omar M Knio, Etienne Besnoin. Numerical study of thermoacoustic heat exchangers in the thin plate limit. *Numerical Heat Transfer, Part A: Applications*, 40(5):445–471, 2001.

[95] Aniruddha S Worlikar. Numerical study of oscillatory flow and heat transfer in a loaded thermoacoustic stack. *Numerical Heat Transfer: Part A: Applications*, 35(1):49–65, 1999.

[96] David Marx and Philippe Blanc-Benon. Numerical simulation of stack-heat exchangers coupling in a thermoacoustic refrigerator. *AIAA journal*, 42(7):1338–1347, 2004.

[97] Etienne Besnoin and Omar M Knio. Numerical study of thermoacoustic heat exchangers. *ACTA Acustica united with Acustica*, 90(3):432–444, 2004.

[98] B. L. Minner, J. E. Braun, and L. Mongeau. Optimizing the design of a thermoacoustic refrigerator. In *International Refrigeration and Air Conditioning Conference*, pages 315–322, 1996.

[99] Konstantin I Matveev, Gregory William Swift, and Scott Backhaus. Temperatures near the interface between an ideal heat exchanger and a thermal buffer tube or pulse tube. *International journal of heat and mass transfer*, 49(5-6):868–878, 2006.

[100] Robert M Keolian and Steven L Garrett. Thermoacoustics: a unifying perspective for some engines and refrigerators. *The Journal of the Acoustical Society of America*, 143(4):2110–2110, 2018.

[101] Accordance Ntimane and Lagouge Tartibu. Impact of heat exchanger length and porosity in a travelling-wave thermo-acoustic engine. In *2023 14th International Conference on Mechanical and Intelligent Manufacturing Technologies (ICMIMT)*, pages 292–298. IEEE, 2023.

[102] Kheira Nehar Belaid and Omar Hireche. Influence of heat exchangers blockage ratio on the performance of thermoacoustic refrigerator. *International Journal of Heat and Mass Transfer*, 127:834–842, 2018.

[103] N Cao, JR Olson, Gregory William Swift, and S Chen. Energy flux density in a thermoacoustic couple. *Journal of the Acoustical Society of America*, 99(6):3456–3464, 1996.

[104] Mohanad Q Kamil, Samir Gh Yahya, and Itimad DJ Azzawi. Design methodology of standing-wave thermoacoustic refrigerator: Theoretical analysis. *International Journal of Air-Conditioning and Refrigeration*, 31(1):7, 2023.

[105] Antonio Piccolo and G Pistone. Estimation of heat transfer coefficients in oscillating flows: The thermoacoustic case. *International Journal of Heat and Mass Transfer*, 49(9-10):1631–1642, 2006.

[106] W Pat Arnott, Henry E Bass, and Richard Raspet. General formulation of thermoacoustics for stacks having arbitrarily shaped pore cross sections. *The Journal of the Acoustical Society of America*, 90(6):3228–3237, 1991.

[107] Ahmed Hamood, Artur J Jaworski, Liam Blunt, and Andrew Townsend. The application of additive manufacturing to heat exchangers for oscillatory flow: A case study. *Proceedings of the Institution of Mechanical Engineers, Part B: Journal of Engineering Manufacture*, page 09544054231199520, 2023.

[108] Xiaoqing Wang, Xibing Gong, and Kevin Chou. Review on powder-bed laser additive manufacturing of inconel 718 parts. *Proceedings of the Institution of Mechanical Engineers, Part B: Journal of Engineering Manufacture*, 231(11):1890–1903, 2017.

[109] Geng Chen, Wang Kai, Liu Liu, Long Gao, Zhaoyu Li, and Lihua Tang. Experimental evaluation of an integrated thermoacoustic stack. *Thermal Science and Engineering Progress*, page 103810, 2025.

[110] Carlo Scalo, Sanjiva K Lele, and Lambertus Hesselink. Linear and nonlinear modelling of a theoretical travelling-wave thermoacoustic heat engine. *Journal of Fluid Mechanics*, 766:368–404, 2015.

[111] Jeffrey Lin, Carlo Scalo, and Lambertus Hesselink. High-fidelity simulation of a standing-wave thermoacoustic–piezoelectric engine. *Journal of Fluid Mechanics*, 808:19–60, 2016.

[112] Mustapha Mahdaoui, Rachid Bennacer, Smaïne Kouidri, and N Martaj. Numerical investigation of thermoacoustic engine using implicit large eddy simulation. In *Proceedings of the 7th European Congress on Computational Methods in Applied Sciences and Engineering, Crete Island, Greece*, pages 5–10, 2016.

[113] Kazuto Kuzuu and Shinya Hasegawa. Numerical investigation of heated gas flow in a thermoacoustic device. *Applied Thermal Engineering*, 110:1283–1293, 2017.

[114] Chou Aw Lin, Fatimah Al Zahrah Mohd Saat, and Fadhilah Shikh Anuar. Heat transfer for the oscillatory flow of thermoacoustics across an in-line tube-banks heat-exchanger. *Heat Transfer Engineering*, 44(10):865–883, 2023.

[115] Erman Aslan, Mert Ozsaban, Guven Ozcelik, and Hasan Riza Guven. A numerical analysis of convection heat transfer and friction factor for oscillating corrugated channel flows. *Heat Transfer Engineering*, 42(3-4):181–190, 2021.

[116] Abdelmaged H Ibrahim, Islam A Ramadan, Hélène Bailliet, and Ehab Abdel-Rahman. Acoustic viscous boundary layer beyond laminar regime: Particle image velocimetry measurements. *International Journal of Heat and Fluid Flow*, 98:109062, 2022.

[117] Islam A Ramadan, Hélène Bailliet, and Jean-Christophe Valière. Experimental investigation of oscillating flow characteristics at the exit of a stacked mesh grid regenerator. *The Journal of the Acoustical Society of America*, 149(2):807–818, 2021.

[118] David Gedeon. *SAGE User's Guide, v13 Edition*, 2025. Accessed: 2025.

[119] Rui Yang, Nathan Blanc, Ariel Vardi-Chouchana, Noam Ouzana, and Guy Z Ramon. Pc-tas: A design environment for phase-change and classical thermoacoustic systems. *SoftwareX*, 19:101142, 2022.

[120] Rodger W. Dyson, Scott D. Wilson, Roy C. Tew, and Rikako Demko. Fast whole-engine stirling analysis. NASA Technical Memorandum NASA/TM—2005-213960, NASA Glenn Research Center, Cleveland, Ohio, 2005. Accessed: 2025-11-03.

[121] Bill Ward, John Clark, and Greg Swift. *Design Environment for Low-amplitude Thermoacoustic Energy Conversion (DeltaEC), Version 6.4b2.9: Users Guide*. Los Alamos National Laboratory, Los Alamos, NM, 2023. For the latest version, visit www.lanl.gov/thermoacoustics. Accessed: 2025-11-03.

[122] Luis A Rodriguez, Rodger Dyson, Mark Wernet, and Ronald Leibach. Thermoacoustic thermal management for electric aircraft. In *AIAA SCITECH 2025 Forum*, page 1477, 2025.

[123] A Di Meglio, N Massarotti, and A Piccolo. Experimental validation of a heat exchanger model for thermoacoustic applications. In *Journal of Physics: Conference Series*, volume 2685, page 012014. IOP Publishing, 2024.

[124] Florian Zink, Jeffrey Vipperman, and Laura Schaefer. Cfd simulation of a thermoacoustic engine with coiled resonator. *International Communications in Heat and Mass Transfer*, 37(3):226–229, 2010.

[125] Umar Nawaz Bhatti, Salem Bashmal, Sikandar Khan, and Rached Ben-Mansour. Numerical modeling and performance evaluation of standing wave thermoacoustic refrigerators with a multi-layered stack. *Energies*, 13(17):4360, 2020.

[126] Umar Nawaz Bhatti, Salem Bashmal, Sikandar Khan, and Rached Ben-Mansour. Numerical modeling of standing wave thermoacoustic devices–a review: Modélisation numérique des dispositifs thermoacoustiques à ondes stationnaires–une revue. *International Journal of Refrigeration*, 146:47–62, 2023.

[127] JA Lycklama à Nijeholt, MEH Tijani, and S Spoelstra. Simulation of a traveling-wave thermoacoustic engine using computational fluid dynamics. *The Journal of the Acoustical Society of America*, 118(4):2265–2270, 2005.

[128] Tadeusz Stolarski, Yuji Nakasone, and Shigeka Yoshimoto. *Engineering analysis with ANSYS software*. Butterworth-Heinemann, 2018.

[129] GY Yu, EC Luo, W Dai, and JY Hu. Study of nonlinear processes of a large experimental thermoacoustic-stirling heat engine by using computational fluid dynamics. *Journal of applied physics*, 102(7), 2007.

[130] Moussa Moindze Ali, Nadia Martaj, Amine Laaouatni, S Savarese, Rachid Bennacer, and Smaîne Kouidri. 2d simulation of the oscillating flow in the thermoacoustic engine swift backhaus. In *2016 International Renewable and Sustainable Energy Conference (IRSEC)*, pages 862–865. IEEE, 2016.

[131] COMSOL Multiphysics. Introduction to comsol multiphysics®. *COMSOL Multiphysics, Burlington, MA, accessed Feb*, 9(2018):32, 1998.

[132] JA Lycklama à Nijeholt, MEH Tijani, S Spoelstra, MS Loginov, and AK Kuczaj. Cfd modeling of streaming phenomena in a torus-shaped thermoacoustic engine. In *Proceedings of the 19th International Congress on Sound and Vibration*, volume 1, pages 1–8, 2012.

[133] Oumayma Miled, Hacen Dhahri, and Abdallah Mhimid. Numerical investigation of porous stack for a solar-powered thermoacoustic refrigerator. *Advances in Mechanical Engineering*, 12(6):1687814020930843, 2020.

[134] Mahathir Rahmany, Elankovan Sundararajan, Abdullah Mohd Zin, and Shahrir Abdullah. Implementation strategy for d2q9 model on desktop grid environment. *Procedia Technology*, 11:1110–1116, 2013.